



# UNIVERSIDAD DE INVESTIGACIÓN DE TECNOLOGÍA EXPERIMENTAL YACHAY

Escuela de Ciencias Físicas y Nanotecnología

## Analytical Tight Binding Hamiltonian for 2D Black Phosphorus

Trabajo de integración curricular presentado como  
requisito para la obtención del título de ingeniero en  
nanotecnología

**Autor:**

Dennis A. Freire

**Tutor:**

Mayra A. Peralta, PhD.  
(Yachay Tech)

**Co-Tutor:**

Francisco Mireles, PhD.  
(CNyN-UNAM)

Urcuquí, Julio del 2021

© Dennis Freire 2021

**SECRETARÍA GENERAL**  
**(Vicerrectorado Académico/Cancillería)**  
**ESCUELA DE CIENCIAS FÍSICAS Y NANOTECNOLOGÍA**  
**CARRERA DE NANOTECNOLOGÍA**  
**ACTA DE DEFENSA No. UITEY-PHY-2021-00015-AD**

A los 22 días del mes de junio de 2021, a las 15:00 horas, de manera virtual mediante videoconferencia, y ante el Tribunal Calificador, integrado por los docentes:

<b>Presidente Tribunal de Defensa</b>	Dr. PINTO ESPARZA, HENRY PAUL , Ph.D.
<b>Miembro No Tutor</b>	Dr. GUEVARA GRANIZO, MARCO VINICIO , Ph.D.
<b>Tutor</b>	Dra. PERALTA ARCIA, MAYRA ALEJANDRA DE JESUS , Ph.D.

El(la) señor(ita) estudiante **FREIRE SOSA, DENNIS ALEJANDRO**, con cédula de identidad No. **0550325468**, de la **ESCUELA DE CIENCIAS FÍSICAS Y NANOTECNOLOGÍA**, de la Carrera de **NANOTECNOLOGÍA**, aprobada por el Consejo de Educación Superior (CES), mediante Resolución **RPC-SO-13-No.156-2015**, realiza a través de videoconferencia, la sustentación de su trabajo de titulación denominado: **ANALYTICAL TIGHT BINDING HAMILTONIAN FOR 2D BLACK PHOSPHORUS**, previa a la obtención del título de **INGENIERO/A EN NANOTECNOLOGÍA**.

El citado trabajo de titulación, fue debidamente aprobado por el(los) docente(s):

<b>Tutor</b>	Dra. PERALTA ARCIA, MAYRA ALEJANDRA DE JESUS , Ph.D.
--------------	--

Y recibió las observaciones de los otros miembros del Tribunal Calificador, las mismas que han sido incorporadas por el(la) estudiante.

Previamente cumplidos los requisitos legales y reglamentarios, el trabajo de titulación fue sustentado por el(la) estudiante y examinado por los miembros del Tribunal Calificador. Escuchada la sustentación del trabajo de titulación a través de videoconferencia, que integró la exposición de el(la) estudiante sobre el contenido de la misma y las preguntas formuladas por los miembros del Tribunal, se califica la sustentación del trabajo de titulación con las siguientes calificaciones:

Tipo	Docente	Calificación
Presidente Tribunal De Defensa	Dr. PINTO ESPARZA, HENRY PAUL , Ph.D.	9,5
Miembro Tribunal De Defensa	Dr. GUEVARA GRANIZO, MARCO VINICIO , Ph.D.	9,5
Tutor	Dra. PERALTA ARCIA, MAYRA ALEJANDRA DE JESUS , Ph.D.	9,9

Lo que da un promedio de: **9.6 (Nueve punto Seis)**, sobre 10 (diez), equivalente a: **APROBADO**

Para constancia de lo actuado, firman los miembros del Tribunal Calificador, el/la estudiante y el/la secretario ad-hoc.

*Certifico que en cumplimiento del Decreto Ejecutivo 1017 de 16 de marzo de 2020, la defensa de trabajo de titulación (o examen de grado modalidad teórico práctica) se realizó vía virtual, por lo que las firmas de los miembros del Tribunal de Defensa de Grado, constan en forma digital.*

**FREIRE SOSA, DENNIS ALEJANDRO**  
**Estudiante**

**Dr. PINTO ESPARZA, HENRY PAUL , Ph.D.**  
**Presidente Tribunal de Defensa**

**HENRY PAUL PINTO ESPARZA**  
 Digitally signed by HENRY PAUL PINTO ESPARZA  
 Date: 2021.06.22 17:28:28 -05'00'

Dra. PERALTA ARCIA, MAYRA ALEJANDRA DE JESUS , Ph.D.  
**Tutor**

MAYRA ALEJANDRA DE JESUS PERALTA ARCIA  
Digitally signed by  
MAYRA ALEJANDRA DE  
JESUS PERALTA ARCIA  
Date: 2021.06.22 16:15:10  
-05'00'

Dr. GUEVARA GRANIZO, MARCO VINICIO , Ph.D.  
**Miembro No Tutor**

MARCO  
VINICIO  
GUEVARA  
GRANIZO  
Firmado  
digitalmente por  
MARCO VINICIO  
GUEVARA GRANIZO  
Fecha: 2021.06.22  
16:22:58 -05'00'

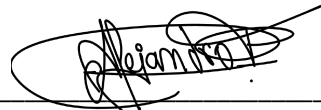
CIFUENTES TAFUR, EVELYN CAROLINA  
**Secretario Ad-hoc**

EVELYN  
CAROLINA  
CIFUENTES TAFUR  
Digitally signed by  
EVELYN CAROLINA  
CIFUENTES TAFUR  
Date: 2021.06.22  
16:10:33 -05'00'

**AUTORÍA**

Yo, **Dennis Alejandro Freire Sosa**, con cédula de identidad 0550325468, declaro que las ideas, juicios, valoraciones, interpretaciones, consultas bibliográficas, definiciones y conceptualizaciones expuestas en el presente trabajo; así cómo, los procedimientos y herramientas utilizadas en la investigación, son de absoluta responsabilidad de el/la autora (a) del trabajo de integración curricular. Así mismo, me acojo a los reglamentos internos de la Universidad de Investigación de Tecnología Experimental Yachay.

Urcuquí, Julio del 2021.



Dennis Alejandro Freire Sosa  
Ci: 0550325468

### AUTORIZACIÓN DE PUBLICACIÓN

Yo, **Dennis Alejandro Freire Sosa**, con cédula de identidad 0550325468, cedo a la Universidad de Investigación de Tecnología Experimental Yachay, los derechos de publicación de la presente obra, sin que deba haber un reconocimiento económico por este concepto. Declaro además que el texto del presente trabajo de titulación no podrá ser cedido a ninguna empresa editorial para su publicación u otros fines, sin contar previamente con la autorización escrita de la Universidad.

Asimismo, autorizo a la Universidad que realice la digitalización y publicación de este trabajo de integración curricular en el repositorio virtual, de conformidad a lo dispuesto en el Art. 144 de la Ley Orgánica de Educación Superior

Urcuquí, Julio del 2021.



Dennis Alejandro Freire Sosa  
CI: 0550325468

*Dedicado a  
mi familia*

# Acknowledgments

First of all, I want to say thank you very much to my advisor: Mayra Peralta, and my co-advisor: Francisco Mireles because without them, the development of this thesis would not have been possible. Second, to the most important person in my life that were with me in all moment and never until now has she left me alone, Allison. Third, I want to thank my family because they where beside to me from the beginning to the end of this stage in my life. Finally, but not less important, to all my friends inside and outside of the University that were with me, giving to me all their support and helping me when I needed always something from them. THANK YOU ALL, THEY MAY BE FEW, BUT THEY ARE THE NECESSARY ONES IN MY LIFE.

# Abstract

Phosphorene, the 2D form of black phosphorus, was first isolated in 2014 by mechanical exfoliation technique. It is known to be the most stable allotrope among the 2D phosphorus group. Its main characteristics shows an anisotropic crystalline structure that leads to anisotropic bands around the  $\Gamma$  point, with a gap of 2 eV, making it a promising material for applications in electronic, optoelectronic, and spintronic devices such as sensors and actuators, among others. Several first-principles calculations have studied the electronic bands for this material. However, it is still not clear yet which hybridizations among different orbitals are responsible for the local density of states (LDOS) and the shape of the bands near the Fermi level. In this work, we have performed a theoretical study of the electronic bands of phosphorene by constructing an analytical tight-binding model based on the Slater and Koster parametrization, and comparing our results with the bands presented in the literature obtained from density functional theory (DFT) calculation. To this end, we design a basis containing a minimum set of four hybrid orbitals corresponding to the four atoms in the primitive lattice of phosphorene. Surprisingly, a minimal basis consisting of a combination of solely  $p_y$  and  $p_z$  orbitals, suffices to reproduce the main features of the band structure at low energies predicted by DFT calculations. Namely, the band asymmetry around the  $\Gamma$  point with a bandgap of 2.19 eV, and the anisotropic shape of the bands around the S point. Furthermore, it is shown by the Löwding transformation method that the addition in the model of the other atomic orbitals of phosphorus does not introduce a significant change in the main characteristics of the lower bands. The latter validates the robustness of our low energy Hamiltonian for phosphorene.

Key words:

Phosphorene, 2D materials, Tight Binding, DFT, Löwding transformation method, Band Gap.



# Resumen

El fosforeno, la forma 2D del fósforo negro, fue descubierto por primera vez en el año 2014 mediante la técnica de exfoliación mecánica. Este material es conocido por ser el alótropo más estable de entre todo el grupo 2D del fósforo. Sus principales características indican una estructura anisotrópica cristalina que da lugar a bandas anisotrópicas alrededor del punto  $\Gamma$ , con una banda prohibida de 2 eV, haciéndolo un material prometedor para aplicaciones en electrónica, optoelectrónica y dispositivos espintrónicos como sensores y actuadores, entre otros. Varios autores han estudiado la estructura de bandas para este material utilizando cálculos de primeros principios. Sin embargo, todavía no se tiene claro, qué hibridaciones entre diferentes orbitales son las responsables de la densidad local de estados (LDOS) y la forma de las bandas cerca del nivel de Fermi. En este trabajo, se ha desarrollado un estudio teórico de las bandas electrónicas del fosforeno a partir de la construcción de un modelo de amarre fuerte basado en la parametrización de Slater y Koster, y comparando nuestros resultados con las bandas presentadas en la literatura obtenidas de los cálculos de la teoría del funcional de la densidad (DFT). Para ello, designamos una base que contiene un conjunto mínimo de orbitales que corresponden a los cuatro átomos en la red primitiva del fosforeno. Sorpresivamente, una base mínima que consiste en una combinación solamente de orbitales  $p_y$  y  $p_z$ , es suficiente para reproducir las principales características de la estructura de bandas a bajas energías predecidas por los cálculos de DFT. Esto es, la asimetría de las bandas alrededor del punto  $\Gamma$  con una banda prohibida de 2.19 eV, y la forma anisotrópica de las bandas alrededor del punto S. Además, encontramos que la adición en el modelo de otros orbitales atómicos del fosforeno, mediante el método de transformación de Löwding, no introduce cambios significativos en las principales características de las bandas a bajas energías. Este último punto, valida la solidez de nuestro Hamiltoniano a bajas energías para el fosforeno.

Palabras clave:

Fosforeno, Materiales 2D, Modelo de Amarre Fuerte, Teoría funcional de la

densidad, Método de transformación de Löwding, Banda prohibida.

# Contents

<b>Acknowledgments</b>	<b>II</b>
<b>Abstract</b>	<b>III</b>
<b>List of figures</b>	<b>VIII</b>
<b>List of tables</b>	<b>XI</b>
<b>1 Introduction</b>	<b>1</b>
1.1 Phosphorene’s crystalline structure . . . . .	2
1.2 Electronic properties of phosphorene . . . . .	5
1.3 Hypothesis . . . . .	8
1.4 Objectives . . . . .	9
1.4.1 General Objective . . . . .	9
1.4.2 Specific Objectives . . . . .	9
<b>2 Methods</b>	<b>10</b>
2.1 Tight Binding method . . . . .	10
2.2 The Slater-Koster and two center approximation . . . . .	12
2.3 Löwding transformation method . . . . .	13
<b>3 Results and discussion</b>	<b>16</b>
3.1 Tight Binding model for Phosphorene . . . . .	16
3.1.1 The basis of $ \phi\rangle$ and $ \theta\rangle$ orbitals . . . . .	16
3.1.2 Effective Hamiltonian with $ \phi\rangle$ orbitals . . . . .	18
3.1.3 Reciprocal Space Hamiltonian with $ \phi\rangle$ orbitals and band structure . . . . .	19
3.1.4 Effective Hamiltonian with $ \phi\rangle$ orbitals perturbed by $ \theta\rangle$ orbitals, and band structure . . . . .	24
3.1.5 Effective Hamiltonian with $ \phi\rangle$ orbitals perturbed by $s$ orbitals, and band structure . . . . .	28

<i>CONTENTS</i>	VII
<b>4 Conclusions and future work</b>	<b>33</b>
<b>A Continuum Hamiltonian around the <math>\Gamma</math> point</b>	<b>35</b>
<b>Bibliography</b>	<b>38</b>

# List of Figures

1.1	Phosphorene crystalline structure. (a) Structure rotated at an arbitrary angle. $\theta$ is the angle with the $\hat{y}$ axis and $\phi$ is the angle with the $\hat{z}$ axis. The interatomic distances are defined by $b_1$ and $b_2$ . The four atoms of the basis are denoted as A, A', B, and B', so $b_1$ is the A – B distance while $b_2$ is the B – B' or the A – A' distance. (b) Side view showing the puckered structure. (c) Top view. The blue rectangle represents the unit cell with lattice parameters $a$ and $b$ , the lattice parameter $c$ is out of the plane in the $\hat{z}$ direction. . . . .	3
1.2	$sp^3$ hybridization of phosphorene. This type of hybridization is formed by mixing one $2s$ -orbital character, and three $2p$ -orbitals, in order to create four hybrid orbitals with similar characteristics, adapted from [29]. . . . .	4
1.3	Reciprocal lattice of phosphorene showing the high symmetry points $\Gamma$ , S, X, and Y at the first Brillouin zone (See Eq. (1.3)).	5
1.4	The DFT band structure of phosphorene along the all symmetry points of the 1st Brillouin zone, adapted from [30]. The high symmetry points are located at S = $\pi(1/b, 1/a)$ , X = $\pi(1/b, 0)$ , Y = $\pi(0, 1/a)$ , and $\Gamma = (0, 0)$ . The rectangle areas enclose the band structure at the vicinity of S and $\Gamma$ points. Around the $\Gamma$ point, there is an asymmetry between $\Gamma - X$ and $\Gamma - Y$ directions. The bands seem to have an approximately linear behavior in the $\Gamma - X$ direction, in contrast to the $\Gamma - Y$ direction, where they are parabolic. . . . .	7
2.1	SK hopping parameters for atomic orbitals. (a) Interaction between s orbitals by a $\sigma$ bond. (b) Interaction between s and p orbitals by a $\sigma$ bond. (c) Interaction between p orbitals by $\pi$ bonds, adapted from [29]. . . . .	13

- 3.1 The basis of rotated  $|\phi\rangle$  and  $|\theta\rangle$  orbitals in phosphorene. (a) Side view of phosphorene where the  $|\phi\rangle$  orbitals of the four atoms of the basis A', A, B, and B', are represented. These orbitals are slightly rotated in the  $yz$  plane, resulting in a combination of  $p_y$  and  $p_z$  orbitals. (b) Top view of phosphorene picturing the  $|\theta\rangle$  orbitals. These orbitals are rotated in the  $xy$  plane, resulting in a combination of  $p_x$  and  $p_y$  orbitals. The orbitals that are in the top layer atoms are colored in green, and the ones in the bottom layer are colorless. The monolayer of phosphorene lies in the  $xy$  plane. . . . . 17
- 3.2 Electronic band structure of phosphorene. (a) Valence and conduction bands around the  $\Gamma$  point in the  $\Gamma - X$  and  $\Gamma - Y$  directions. (b) Valence and conduction bands around the S point in the  $S - \Gamma$  and  $S - X$  directions. In both cases, the blue (-dashed-) lines are quadratic fits of the DFT bands taken from [30], and the magenta (solid) lines are the eigenvalues from Eqs. (3.13), (3.16), and (3.17), given by our tight-binding model with  $|\phi\rangle$  orbitals from Eq. (3.11). . . . . 23
- 3.3 Band structure of phosphorene with  $|\phi\rangle$  orbitals perturbed by  $|\theta\rangle$  orbitals. (a) Valence and conduction bands around  $\Gamma$  point in the  $X - \Gamma - Y$  directions. (b) Valence and conduction bands around the S point in the  $\Gamma - S - X$  directions. In both cases, the blue (-dashed-) lines represent the DFT fitting taken from [30], and the magenta (solid) lines represent the eigenvalues obtained by our tight-binding model from Eq. (3.24). . . . . 28
- 3.4 Band structure of phosphorene with  $|\phi\rangle$  orbitals perturbed by  $s$  orbitals. (a) Valence and conduction bands around  $\Gamma$  point in the  $X - \Gamma - Y$  directions. (b) Valence and conduction bands around the S point in the  $\Gamma - S - X$  directions. In both cases, the blue (-dashed-) lines represent the DFT fitting taken from [30], and the magenta (solid) lines represent the eigenvalues obtained by our tight-binding model from Eq. (3.31). . . . . 32

- A.1 Electronic band structure of phosphorene around the  $\Gamma$  point from 0 to 1 in  $\mathbf{k}$ . Valence and conduction bands around the  $\Gamma$  point in the  $\Gamma - X$  and  $\Gamma - Y$  directions. The blue (-dashed-) lines are quadratic fits of the DFT bands taken from [30], the magenta (solid) lines are the eigenvalues from Eq. (3.13) given by our tight-binding model with  $|\phi\rangle$  orbitals from Eq. (3.11), and the yellow (dotted) lines are the eigenvalues from the first and the last equations from Eq. (A.3) obtained from the continuum Hamiltonian from Eq. (A.2). . . . . 37

# List of Tables

1.1	Table with the DFT parameters of Phosphorene to be used in this work, taken from [34], and the experimental parameters for black phosphorus, taken from [29]. The interatomic distances are defined by $b_1$ and $b_2$ in angstroms. The four atoms of the basis are denoted as A, A', B, and B' (see Fig. 1.1a), so $b_1$ is the A – B distance while $b_2$ is the B – B' or the A – A' distance. $\theta$ is the angle with the $\hat{y}$ axis, and $\phi$ is the angle with the $\hat{z}$ axis, both in degrees. The lattice parameters are defined by $a$ , and $b$ in angstroms. The bandgap for 2D phoshorene and Bulk Black Phosphorus (BP) is defined in electronvolts. . . . .	6
2.1	SK constants for the energy integral calculations used in this work. The $V_{ss\sigma}$ ( $V_{pp\sigma}$ ) represent the hopping parameters between $s - s$ ( $p - p$ ) orbitals with a $\sigma$ bond. The $V_{sp\sigma}$ represent the hopping parameter between $s - p$ orbitals with a $\sigma$ bond. The $V_{pp\pi}$ represent the hopping parameter between $p - p$ orbitals with a $\pi$ bond (see Fig.2.1). We use the indexes $i=\{x, y, z\}$ and $j=\{x, y, z\}$ for representing the direction of the orbitals, following the rule $i \neq j$ . The $n$ represents the respective cosine directors that are expressed in Eq.(1.2). . . . .	14
3.1	Coupling integrals, at first neighbors, between the $ \phi\rangle$ orbitals of the four atoms of the basis of phosphorene. The reference of energy has been taken at $\varepsilon_p = 0$ . . . . .	18
3.2	Table with the Slater and Koster parameters obtained from the fitting with the DFT bands from [30], for the model of $ \phi\rangle$ orbitals. $V_{pp\sigma}$ and $V_{pp\pi}$ are the SK parameters for hopping between $p_z$ and $p_y$ orbitals forming $\sigma$ and $\pi$ bonds respectively. $V_{AB}$ is the hopping parameter between A(A') and B(B') atoms (see Eq.3.4). . . . .	21



3.3	Table with numerical values of $\alpha$ , $\beta$ , and $\gamma$ expressed in Eq. (3.14). These values were obtained from the tight-binding parameters from Table. 3.2. . . . .	21
3.4	Table with numerical values of the effective masses in $\Gamma - X$ and $\Gamma - Y$ directions calculated from Eq. (3.15) and compared with reference [36]. Our values has been normalized by the rest mass of the electron. . . . .	22
3.5	Hopping and onsite integrals, at first neighbors, between the $ \theta\rangle$ orbitals of the four atoms of the basis of phosphorene. The reference of energy has been taken at $\varepsilon_p = 0$ . . . . .	25
3.6	Overlap integrals, at first neighbors, between the $ \phi\rangle$ and $ \theta\rangle$ orbitals of the four atoms of the basis of phosphorene. The reference of energy has been taken at $\varepsilon_p = 0$ . . . . .	26
3.7	Table with the Slater and Koster parameters obtained from the fitting with the DFT bands, for the model of $ \phi\rangle$ perturbed by $ \theta\rangle$ orbitals. Where $V_{pp\sigma}$ and $V_{pp\pi}$ are the SK parameters for the hopping between $p$ orbitals forming $\sigma$ or $\pi$ bonds. $V_{AB}$ is the hopping parameter between $ \phi\rangle$ orbitals of the A(A') and B(B') atoms (see Eq. (3.4)), and $V_{AA}$ is the hopping parameter between $ \theta\rangle$ orbitals of the A(B) and A'(B'), atoms (see Eq. (3.19)). . . . .	27
3.8	Hopping and onsite integrals, at first neighbors, between the $s$ orbitals of the four atoms of the basis of phosphorene. . . . .	29
3.9	Transfer integral matrix, at first neighbors, between the $ \phi\rangle$ and $s$ orbitals of the four atoms of the basis of phosphorene. The reference of energy has been taken at $\varepsilon_p = 0$ . . . . .	30
3.10	Table with the Tigh-Binding parameters used for the adjustment with the DFT bands, for the model of $ \phi\rangle$ perturbed by $s$ orbitals. Where $V_{sp\sigma}$ , $V_{ss\sigma}$ , $\varepsilon_{sp}$ , $V_{pp\sigma}$ , and $V_{pp\pi}$ represents the SK parameters used for the calculation of the hopping integrals. . . . .	31

# Chapter 1

## Introduction

The study of 2D materials has become very significant since the discovery of graphene in 2004. Graphene is a material that crystallizes in a hexagonal 2D honeycomb structure; it is made up of carbon atoms linked together by covalent bonds, with an  $sp^2$  hybridization. Some of the unique characteristics of this material are a zero band-gap [1, 2], ultra-high carrier mobilities, its tunable electrical behavior [3], and high-temperature superconductivity in twisted bilayer graphene [4]. Since the discovery of the properties of graphene, numerous studies began to be carried out involving other 2D layered materials (2DLM) such as transition metal dichalcogenides (TMDs) like  $MoSe_2$ ,  $MoTe_2$ ,  $WS_2$ ,  $WSe_2$ , and  $TiS_2$ ; gallium selenide (GaSe), Hexagonal Boron Nitride (h-BN), perovskites [1], silicene, and more recently 2D phosphorus [3]. Due to the ultra-thin layer form of 2D materials, their more remarkable properties are: large light-matter interaction, strong nonlinear optical response, strong interlayer coupling, large mechanical strength, high thermal conductivity, and ultrafast carrier dynamics, among others [1, 5, 6], these properties make them very good candidates for potential applications such as catalysis, electronics and photonics [7], power limiters [1, 8], THz wave generation [3, 9], and ultra-thin light sources [10, 11].

Elemental phosphorus can exist in four main allotropic forms, named: red, white, violet, and black phosphorus, depending upon the very different structures and properties [12]. White phosphorus is the most reactive, volatile, and toxic allotrope, formed by 4 phosphorus atoms arranged in a tetrahedral  $P_4$  structure and containing two variants, an  $\alpha$  form, which is fcc, and a  $\beta$  form, with a hexagonal structure [13]. Red phosphorus is more stable than white phosphorus, with an amorphous lattice, and can be synthesized from white phosphorus at temperatures of 525-550 K [13]. Violet phosphorus, like red phosphorus, has an amorphous structure and can be synthesized by chemical vapor deposition (CVD) using amorphous red phos-

phorus [14]. Black phosphorus, on the other hand, is the most stable and least reactive of all the allotropes of phosphorus. This is due to its highly stable layered crystal structure formed by single atomic species, it has an orthorhombic structure, and can be synthesized by heating white phosphorus at high pressure (12.000 atmospheres) in the presence of a catalyst [15].

In black phosphorus, the layers are linked to each other by weak Van der Waals (vdWs) inter-layer interactions with a separation of 3.21 Å to 3.73 Å [4, 16], while in each layer there are phosphorus atoms bonded to each other by covalent bonds [17]. This bulk material has a semiconductor behavior with a tiny band-gap, of about 0.3 eV, which increases with the number of atomic layers [18, 19]. This thickness-dependent band-gap makes it a good candidate in diverse applications like field-effect transistors (FETs) [20], phosphorus based nanomaterials [17, 21], optoelectronic devices [21], and superconductivity [22, 23].

Phosphorene, also known as monolayer black phosphorus, was synthesized for the first time in 2014 through the celebrated method known as the scotch-tape-based micro-cleavage approach [17, 20, 24], which essentially consists of a repetitive peeling of the bulk material until obtaining one or few layers of it. Another method to synthesize phosphorene was reported in [16] by using plasma etching. Among the most remarkable properties of phosphorene are: an experimentally measured band-gap of about 2 eV [25, 26], which makes it a semiconductor material; it has a high anisotropic band structure, of great advantage for several applications for instance in the optical spectrum for the absorption and reflection of light along its lattice arm-chair direction [18, 27]. The charge transport in phosphorene multilayers is one of the most studied characteristics, it depends on its number of layers, for example, the charge mobility increases with the increase of layers reaching values of up to ( $1000 \text{ cm}^2\text{V}^{-1}\text{s}^{-1}$ ) [16]. Also, it has been shown that this material behaves as a superconductor with critical temperatures  $T_c$  between 9.5-10.7 K, and high pressures of about 30 GPa [27]. Finally, but not less important, it has the unusual behavior of having negative Poissons's ratio and an anisotropic Young Modulus [4, 18] [3,13]. All of these properties have allowed phosphorene to be considered for the development of applications in electronic devices such as field-effect transistors, photodetectors, and its use in optics, electronics, photonics, photovoltaics, and spintronics [1, 27, 28].

## 1.1 Phosphorene's crystalline structure

Phosphorene has an orthorhombic primitive lattice, that in 2D can be seen as a rectangular lattice, having a structure that is *armchair* along the  $\hat{y}$  axis and

*zigzag* along the  $\hat{x}$  axis, as shown in Fig. 1.1a and 1.1c. Out of the plane, the puckered structure seems to be a bilayer configuration due to the positions of the atoms (see Fig. 1.1b). In this material, the basis is formed by four atoms, that in the plane are bonded to each other by covalent  $\sigma$  bonds, and out of the plane, by  $\pi$  bonds, forming an  $sp^3$  hybridization (see Fig. 1.2, [29]). The primitive lattice vectors in monolayer phosphorene for the 2D rectangular structure are:

$$\mathbf{a}_1 = b\hat{x}, \quad \mathbf{a}_2 = a\hat{y}, \quad (1.1)$$

where  $b$  and  $a$  are the lattice parameters in the  $\hat{x}$  and  $\hat{y}$  directions respectively (Fig 1.1c).

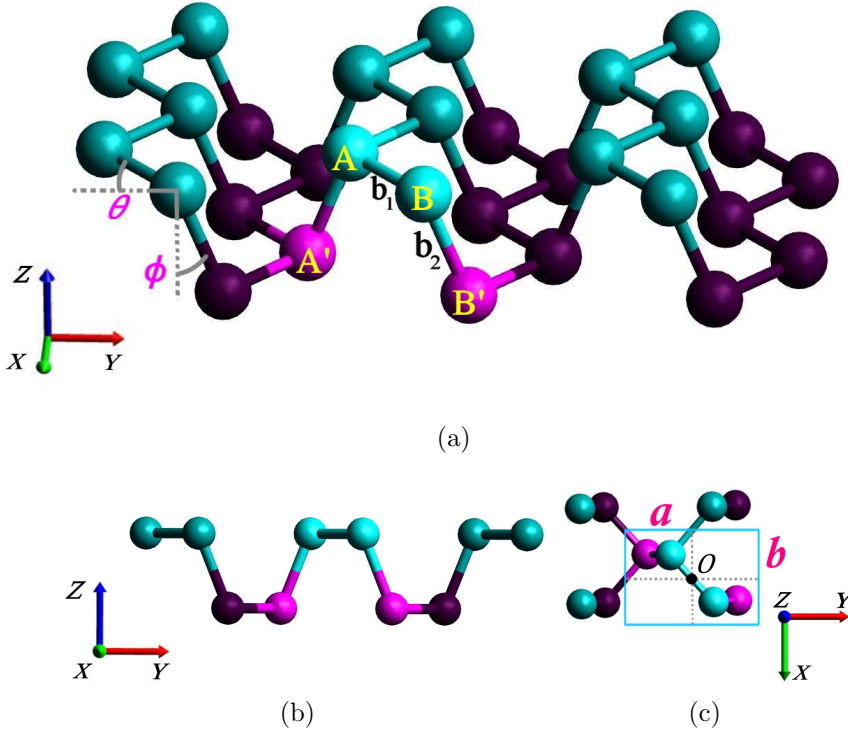


Figure 1.1: Phosphorene crystalline structure. (a) Structure rotated at an arbitrary angle.  $\theta$  is the angle with the  $\hat{y}$  axis and  $\phi$  is the angle with the  $\hat{z}$  axis. The interatomic distances are defined by  $b_1$  and  $b_2$ . The four atoms of the basis are denoted as A, A', B, and B', so  $b_1$  is the A – B distance while  $b_2$  is the B – B' or the A – A' distance. (b) Side view showing the puckered structure. (c) Top view. The blue rectangle represents the unit cell with lattice parameters  $a$  and  $b$ , the lattice parameter  $c$  is out of the plane in the  $\hat{z}$  direction.

The four atoms of the basis are labeled with the letters A, A', B, and B', as shown in Fig. 1.1a. The distances between these atoms can be written as:

$$\begin{aligned}
 \delta_{AB_1} &= b_1 (\pm \sin(\theta), \cos(\theta), 0) = b_1(n_{lx}, n_{ly}, 0), \\
 \delta_{A'B'_1} &= b_1 (\pm \sin(\theta), -\cos(\theta), 0) = b_1(n_{lx}, -n_{ly}, 0), \\
 \delta_{AA'} &= b_2 (0, -\sin(\phi), -\cos(\phi)) = b_2(0, n_y, n_z), \\
 \delta_{BB'} &= b_2 (0, \sin(\phi), -\cos(\phi)) = b_2(0, -n_y, n_z),
 \end{aligned} \tag{1.2}$$

where  $\theta$  and  $\phi$  are the angles with  $\hat{y}$  and  $\hat{z}$  respectively,  $b_1$  is the A-B and A'-B' distance, and  $b_2$  is the A-A' and B-B' distance, as defined in Fig. 1.1a. The values of all the mentioned parameters can be seen in Table 1.1. The sub-index  $l$  is used to distinguish between the two first neighbors B(B') of the atom A(A'), and  $n_{lx}$ ,  $n_{ly}$ ,  $n_y$ , and  $n_z$  are the respective direction cosines.

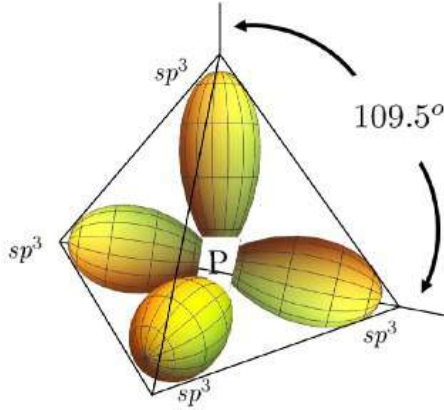


Figure 1.2:  $sp^3$  hybridization of phosphorene. This type of hybridization is formed by mixing one  $2s$ -orbital character, and three  $2p$ -orbitals, in order to create four hybrid orbitals with similar characteristics, adapted from [29].

The 2D reciprocal lattice of phosphorene is also orthorhombic. The 1st Brillouin zone in 2D (figure 1.3) has a rectangular shape with the high symmetry points S, X, Y, and  $\Gamma$ , located at:

$$\begin{aligned}
 S &= \pi \left( \frac{1}{b}, \frac{1}{a} \right), & X &= \pi \left( \frac{1}{b}, 0 \right), \\
 Y &= \pi \left( 0, \frac{1}{a} \right), & \Gamma &= (0, 0).
 \end{aligned} \tag{1.3}$$

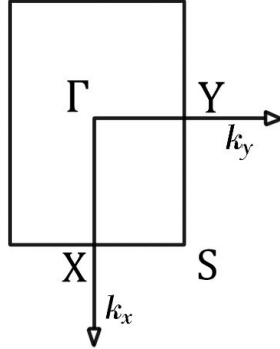


Figure 1.3: Reciprocal lattice of phosphorene showing the high symmetry points  $\Gamma$ , S, X, and Y at the first Brillouin zone (See Eq. (1.3)).

## 1.2 Electronic properties of phosphorene

Among the numerical methods used to model the band structure of phosphorene, we have full-potential linearized augmented plane-wave [30], the Gaussian Plane Waves (GPW) [18, 31], the approximation of one body Green's function, the dynamically screened Coulomb interaction (GWA) [4, 18], and the pseudo-atomic orbital basis [32]; all of these mostly, first-principle calculations based in DFT [18, 24, 31, 33, 32]. By studying the electronic properties with these techniques, it has been possible to find: the excitonic properties [18], the minima and maxima of the conduction and valence bands [18], the bonding between atoms [24], the band structure [24], equilibrium geometry [24], bonding [24], the density of states [30], the contribution of atomic orbitals to each band [30], structural properties [32], and the charge mobility among others characteristics [18, 24, 33, 31, 32].

The characteristic band structure of phosphorene presents the minimum and maximum between the conduction and valence bands around the  $\Gamma$  point [4, 24, 33], where the calculated band-gap varies between 0.8 to 2.17eV, depending on the method used [4, 18, 24, 33, 30, 34]. Also at this point, an anisotropic behavior in the dispersion is observed (see the right rectangle enclosed area in Fig. 1.4). The bands seem to have an approximately linear behavior in the  $k_x$  direction, in contrast to the  $k_y$  direction, where they are parabolic (see Fig. 1.4) [30, 4]. This can be explained also in terms of the effective masses, in the  $k_x$  direction the second derivative of the energy seems to be closer to zero (dispersionless), while along  $k_y$  direction is not (dispersive). The contribution of atomic orbitals for the valence and conduction bands near the  $\Gamma$  and S points is mostly of  $p_z$  character with a small contribution of  $p_y$  orbitals [32, 30]. Finally, but not less important, the dominant

Table 1.1: Table with the DFT parameters of Phosphorene to be used in this work, taken from [34], and the experimental parameters for black phosphorus, taken from [29]. The interatomic distances are defined by  $b_1$  and  $b_2$  in angstroms. The four atoms of the basis are denoted as A, A', B, and B' (see Fig. 1.1a), so  $b_1$  is the A – B distance while  $b_2$  is the B – B' or the A – A' distance.  $\theta$  is the angle with the  $\hat{y}$  axis, and  $\phi$  is the angle with the  $\hat{z}$  axis, both in degrees. The lattice parameters are defined by  $a$ , and  $b$  in angstroms. The bandgap for 2D phosphorene and Bulk Black Phosphorus (BP) is defined in electronvolts.

Parameters	2D Phosphorene (DFT) [30]	Bulk BP (Exp.) [19]
$b_1[\text{\AA}]$	2.243	2.22
$b_2[\text{\AA}]$	2.261	2.24
$\theta$	48.41°	48.17°
$\phi$	21.41°	20.46°
$a[\text{\AA}]$	4.626	4.376
$b[\text{\AA}]$	3.356	3.313
bandgap [eV]	2.17	0.3 (Bulk) - 2.05 (2D)[25]

spin-orbit coupling around the  $\Gamma$  point is of the Rashba kind, with a splitting of around  $2 \mu\text{eV}$ , while around the S point, the dominant spin-orbit coupling is of the intrinsic kind with a splitting of about 20 meV [4, 24].

The use of analytical methods plays an important role in the study of electronic properties because they provide detailed information about the band structure of phosphorene. For example, it can be calculated the hopping and overlapping integrals centered at different atomic sites [32, 35], in a way that a more complete explanation of the relation between the shape of the bands and the atomic structure, the symmetries of the material, and the hybridization between atoms, can be provided [36]. Very useful methods for making analytical models in phosphorene are Tight-Binding (TB) [37, 32] and the  $k \cdot p$  Theory [36, 38]. In the case of the TB method, the electronic structure is described along the full Brillouin zone by a set of wave functions based on the superposition of the atomic orbitals of each atom as Bloch functions, on the other hand, the  $k \cdot p$  method is an approximation to calculate the electronic structure around the vicinity of a selected point from the Brillouin zone.

Among the most relevant studies involving analytical methods in phosphorene, we highlight: Menezes *et. al.* [32], who presented a numerical tight-binding model with adjustable Slater and Koster parameters, with and

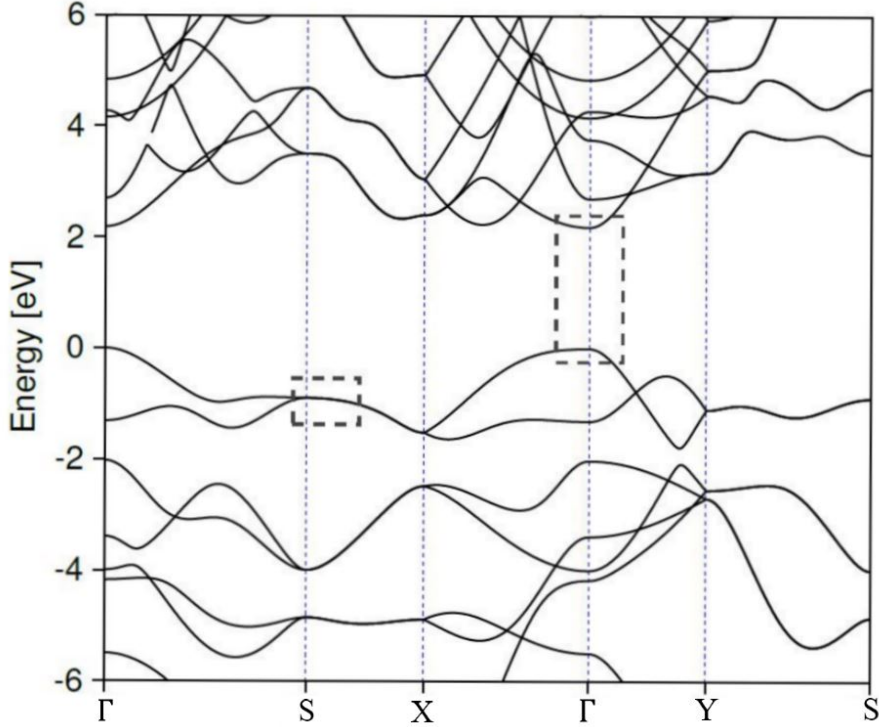


Figure 1.4: The DFT band structure of phosphorene along the all symmetry points of the 1st Brillouin zone, adapted from [30]. The high symmetry points are located at  $S = \pi(1/b, 1/a)$ ,  $X = \pi(1/b, 0)$ ,  $Y = \pi(0, 1/a)$ , and  $\Gamma = (0, 0)$ . The rectangle areas enclose the band structure at the vicinity of S and  $\Gamma$  points. Around the  $\Gamma$  point, there is an asymmetry between  $\Gamma - X$  and  $\Gamma - Y$  directions. The bands seem to have an approximately linear behavior in the  $\Gamma - X$  direction, in contrast to the  $\Gamma - Y$  direction, where they are parabolic.

without taking into account the overlap matrix, having as a result that the model that includes the overlaps gives a better parametrization to adjust the bands in phosphorene. But without devilling on the nature of the low energy Hamiltonians at the high symmetry points. Fukuoka *et. al.* [37], proposed a  $16 \times 16$  linear combination of atomic orbitals (LCAO) Hamiltonian to model the bands of phosphorene at low energies, providing only a qualitative description where they asserted the DFT calculations. Kafei *et. al.* [38], also developed a  $16 \times 16$   $k \cdot p$  Hamiltonian for bands at low energies considering all couplings between atoms up to second-order correction, being linear in one direction and non linear in the other direction, in this work, the authors obtained a good approximation to the electronic bands considering that the off-diagonal elements of the Hamiltonian must be of second order in



the wavenumber. Popovic *et. al.* [35], proposed a TB model of  $p_z$  rotated orbitals with a small contribution of  $p_y$  orbitals with only two hopping effective parameters, with this, the authors obtained the bands around the  $\Gamma$  point at low energies with sufficient accuracy compared with the DFT model. Finally, Jaroslav *et. al.* [36], developed a  $k \cdot p$  Hamiltonian model for 4 and 6 bands, and they fit the analytical model with first-principles calculations, asserting the anisotropy of the bands of phosphorene around the  $\Gamma$  point.

In spite of all the models described above, a simplified analytical Hamiltonian for phosphorene, where the role of the overlaps between the atomic orbitals could be included in the hopping parameters, is still missing. In this work, we have developed a tight-binding model to address this problem. With this goal, we have chosen a basis of tilted orbitals with components  $p_z$  and  $p_y$  as in reference [35], but with the inclusion of the specific overlaps between the orbitals of different atoms, by using the Slater and Koster approximation to calculate the matrix relevant elements of the Hamiltonian. With this simple analytical model, we have reproduced the main characteristics of the bands around the high symmetry points of the first Brillouin zone  $\Gamma$  and S, also, we have found the effective masses in the  $\Gamma - X$  and the  $\Gamma - Y$  directions, in terms of the hybridizations between orbitals of the atoms of the basis of phosphorene.

The structure of this manuscript is as follows: in Chapter 2 we present the methods that support this work, which are: the tight-binding method, the Slater Koster and the two center approximation, and the Löwding transformation method. In Chapter 3, we present our results with a discussion particularly on the role of the overlapping terms that mostly contribute to the band behavior, comparing always with the results of the DFT model of reference [30]. Finally, in Chapter 4, we present the conclusion of this work.

### 1.3 Hypothesis

An analytical tight-binding model, based on the Slater and Koster two centers approximation and with a basis of rotated  $|\phi\rangle$  (combination of  $p_y$  and  $p_z$ ) and  $|\theta\rangle$  (combination of  $p_x$  and  $p_y$ ) orbitals, can be developed to find a minimal Hamiltonian for phosphorene that contains the relevant information of the hybridizations between orbitals that give origin to its anisotropic band structure around the  $\Gamma$  and S points close to the Fermi energy.

## 1.4 Objectives

### 1.4.1 General Objective

To develop an analytical tight-binding Hamiltonian for 2D Black phosphorus valid for the high symmetry points S and  $\Gamma$  near the Fermi energy.

### 1.4.2 Specific Objectives

- To construct a basis of rotated orbitals  $|\phi\rangle$  and  $|\theta\rangle$  for phosphorene.
- To derive an effective Hamiltonian in the direct space for the basis of  $|\phi\rangle$  orbitals.
- To determine by Fourier transform the Hamiltonian in reciprocal space.
- From the Hamiltonian obtained in the previous point, to obtain the band structure in the vicinity of the high symmetry points S and  $\Gamma$ .
- To compare the band structure obtained with our model with those reported in the literature by first principle calculations.
- To make a perturbation study of the influence of the  $|\theta\rangle$  and  $s$  orbitals in the model described previously.

# Chapter 2

## Methods

Wigner and Seitz were the pioneers in the study of band calculations in crystalline materials in solid-state physics. The first calculations were developed from the study of the wave-function, where the methodology they used is summarized in three methods; The Wigner-Seitz method, very useful for the understanding of alkali metals [39]; the Pseudopotential method, used for the study of metals [39]; and the Tight Binding method (TB), used to the study of solids, semiconductors and 2D-dimensional materials [40, 41].

The TB method or Linear Combination of Atomic Orbitals (LCAO) was first introduced in 1928 by Felix Bloch who proposed the quantum theory of solids. This method is a mathematical model that studies the electrons that are tightly bonded to the nuclei of the atoms. As the name indicates, it consists of taking the wave function of the electrons as a linear combination of the atomic orbitals of the free atoms that constitute the solid material [40, 39, 42]. TB provides information about the electronic and transport properties, of crystalline solid systems that are composed of many atoms [40, 41].

### 2.1 Tight Binding method

This section is supported by [43, 42, 44]. The model starts defining electronic Bloch states  $\Phi(\mathbf{k}, \mathbf{r})$  that depend on the position vector  $\mathbf{r}$ , and a wave vector  $\mathbf{k}$  of the electron. These functions are constructed for a system of  $n$  atomic localized orbitals  $\phi_u$  (Wannier Functions) using one atom in each unit cell, labeled by the index  $u = 1, \dots, n$ , and can be written as:

$$\Phi_u(\mathbf{k}, \mathbf{r}) = \frac{1}{\sqrt{N}} \sum_{v=1}^N e^{i\mathbf{k} \cdot \mathbf{R}_{u,v}} \phi_u(\mathbf{r} - \mathbf{R}_{u,v}), \quad (2.1)$$

where the sum is over  $N$  unit cells, that can be labeled by  $v = 1, \dots, N$  and  $\mathbf{R}_{u,v}$  represents the position of the  $u$ th orbital in the  $v$ th unit cell.

We can express the electronic wave function  $\Psi_l(\mathbf{k}, \mathbf{r})$  that depends on a linear superposition of the  $n$  different Bloch functions

$$\Psi_l(\mathbf{k}, \mathbf{r}) = \sum_{u=1}^n c_{l,u}(\mathbf{k}) \Phi_u(\mathbf{k}, \mathbf{r}), \quad (2.2)$$

where  $c_{l,u}$  are the expansion coefficients. The energy values  $\varepsilon_l(k)$  of the  $l$ th energy band are given by

$$\varepsilon_l(\mathbf{k}) = \frac{\langle \Psi_l | \hat{H} | \Psi_l \rangle}{\langle \Psi_l | \Psi_l \rangle}, \quad (2.3)$$

where  $\hat{H}$  is the Hamiltonian operator. Now, substituting the expansion of the wave function (2.2) into the equation of energy (2.3) we obtain

$$\varepsilon_l(\mathbf{k}) = \frac{\sum_{v,u}^n c_{lv}^* c_{lu} \langle \Phi_v | \hat{H} | \Phi_u \rangle}{\sum_{v,u}^n c_{lv}^* c_{lu} \langle \Phi_v | \Phi_u \rangle} = \frac{\sum_{v,u}^n c_{lv}^* c_{lu} H_{vu}}{\sum_{v,u}^n c_{lv}^* c_{lu} S_{vu}}, \quad (2.4)$$

where  $H_{vu} = \langle \Phi_v | \hat{H} | \Phi_u \rangle$  represents the transfer integral matrix and  $S_{vu} = \langle \Phi_v | \Phi_u \rangle$  represents the overlap integral matrix. In order to minimize the energy  $\varepsilon_l$ , we shall apply the first partial derivative of  $\varepsilon_l$  with respect to the coefficient  $c_{lv}^*$ , to obtain

$$\frac{\partial \varepsilon_l}{\partial c_{lv}^*} = \frac{\sum_u^n c_{lu} H_{vu}}{\sum_{v,u}^n c_{lv}^* c_{lu} S_{vu}} - \frac{\sum_{v,u}^n c_{lv}^* c_{lu} H_{vu} \sum_u^n c_{lu} S_{vu}}{(\sum_{v,u}^n c_{lv}^* c_{lu} S_{vu})^2}, \quad (2.5)$$

and making  $(\partial \varepsilon_l / \partial c_{lv}^* = 0)$

$$\sum_{u=1}^n c_{ul} H_{vu} = \varepsilon_l \sum_{u=1}^n c_{lu} S_{vu}. \quad (2.6)$$

For general values of  $n$ , the transfer integral matrix  $H$ , the overlap integral matrix  $S$ , and the expansion coefficients  $\psi_l$ , as a column vector, are

$$H = \begin{pmatrix} H_{11} & H_{12} & \cdots & H_{1n} \\ H_{21} & H_{22} & \cdots & H_{2n} \\ \vdots & \vdots & \ddots & \vdots \\ H_{n1} & H_{n2} & \cdots & H_{nn} \end{pmatrix}, \quad S = \begin{pmatrix} S_{11} & S_{12} & \cdots & S_{1n} \\ S_{21} & S_{22} & \cdots & S_{2n} \\ \vdots & \vdots & \ddots & \vdots \\ S_{n1} & S_{n2} & \cdots & S_{nn} \end{pmatrix}, \quad \psi_l = \begin{pmatrix} c_{l1} \\ c_{l2} \\ \vdots \\ c_{ln} \end{pmatrix}. \quad (2.7)$$

The equation (2.6) can be written as

$$H\psi_l = \varepsilon_l S\psi_l. \quad (2.8)$$

Calculating the determinant of the system (2.8)

$$\det(H - \varepsilon_l S) = 0, \quad (2.9)$$

will give us the respective eigenvalues  $\varepsilon_l$  that describe the band structure of the material. The number of eigenvalues calculated is according to  $l$ , which represents the number of the different atomic orbitals of each unit cell  $v$ .

## 2.2 The Slater-Koster and two center approximation

The TB method, as mentioned before in Sec. 2.1, involves the calculation of the transfer integral matrix  $H$  in Eq. (2.7), in which each of the elements is given by an integral of the form:

$$H_{op} = \langle \Phi_o | \hat{H} | \Phi_p \rangle = \int \Phi_o^*(\mathbf{r} - \mathbf{R}_o) \hat{H} \Phi_p(\mathbf{r} - \mathbf{R}_p) dr, \quad (2.10)$$

where  $\Phi_{o,p}$  represents the orbital contribution of the atom at position  $\mathbf{R}_{o,p}$ . The Hamiltonian operator  $\hat{H}$  is:

$$\hat{H} = -\frac{\hbar^2}{2m} \nabla^2 + \sum_{\mathbf{R}_i} V_{at}(\mathbf{r} - \mathbf{R}_i), \quad (2.11)$$

being the first term the kinetic contribution, and the second term the atomic potential, where  $\mathbf{r}$  is the position of the electron and  $\mathbf{R}_i$  is the position of the atoms in the crystal.

The potential  $V_{at}(\mathbf{r})$  in Eq. (2.11), is an atomic potential that contains all the contributions of the lattice atoms. This makes that the integrals in Eq. (2.10) depend on multiple atomic positions. For solving this problem, Slater and Koster in their work [40], proposed a solution that consists in approximate the atomic potential, taking into account only the interaction between two atoms, the source atom, and the target atom so, the atomic potential in Eq. (2.11) is replaced by the expression:

$$V(\mathbf{r}) = \sum_{o,p} V_{at}(\mathbf{R}_p - \mathbf{R}_o). \quad (2.12)$$

given this approximation, the integrals from Eq. (2.10) can be replaced by combinations of SK parameters [40]. According to the Slater and Koster notation in Table. 2.1, the first two subindices in the symbols  $V_{(abc)}$ , represent the two type orbitals involved in the hopping ( $s, p, d$ ), and the sub-index  $c$ , is the type of bond that joins them ( $\sigma, \pi, \delta$ ). A schematic representation of how the bonds  $\sigma$  and  $\pi$  looks like joining the orbitals is presented in Fig. 2.1.

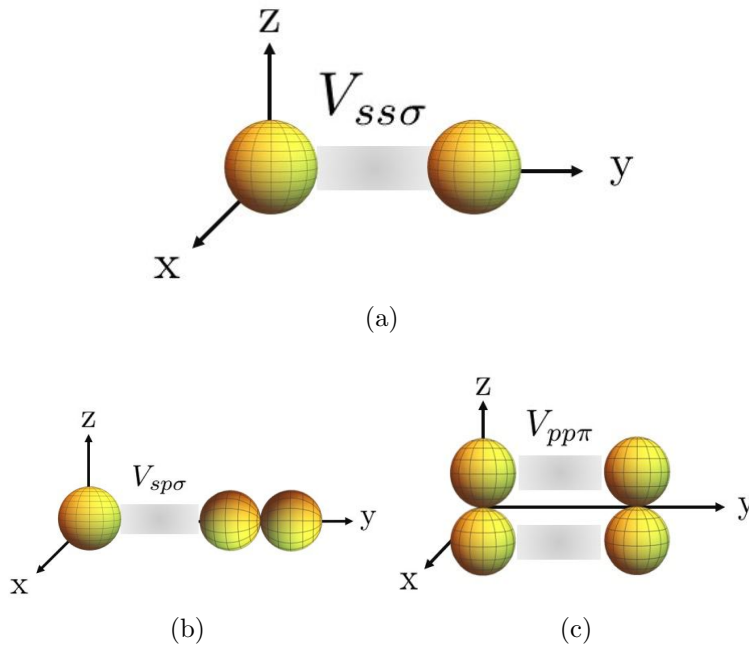


Figure 2.1: SK hopping parameters for atomic orbitals. (a) Interaction between s orbitals by a  $\sigma$  bond. (b) Interaction between s and p orbitals by a  $\sigma$  bond. (c) Interaction between p orbitals by  $\pi$  bonds, adapted from [29].

## 2.3 Löwding transformation method

The Löwding partitioning technique is used in perturbative quantum theory as a powerful technique for solving eigenvalues problems, this is because it does not distinguish between non-degenerated and degenerated states, providing a simplified solution as an approximation to a more complex problem [45]. In this technique, an approach to construct effective Hamiltonians from sub-matrices that seek to perturb the main matrix is defined.

The full Hamiltonian  $H$  of the entire system, shall be written as a partition of four blocks of submatrices that depend on two different subspaces  $H_0$

Table 2.1: SK constants for the energy integral calculations used in this work. The  $V_{ss\sigma}$  ( $V_{pp\sigma}$ ) represent the hopping parameters between  $s-s$  ( $p-p$ ) orbitals with a  $\sigma$  bond. The  $V_{sp\sigma}$  represent the hopping parameter between  $s-p$  orbitals with a  $\sigma$  bond. The  $V_{pp\pi}$  represent the hopping parameter between  $p-p$  orbitals with a  $\pi$  bond (see Fig. 2.1). We use the indexes  $i=\{x, y, z\}$  and  $j=\{x, y, z\}$  for representing the direction of the orbitals, following the rule  $i \neq j$ . The  $n$  represents the respective cosine directors that are expressed in Eq. (1.2).

$\langle s \hat{H} s\rangle$	$V_{ss\sigma}$
$\langle s \hat{H} p_i\rangle$	$n_i V_{sp\sigma}$
$\langle p_i \hat{H} p_i\rangle$	$n_i^2 V_{pp\sigma} + (1 - n_i^2) V_{pp\pi}$
$\langle p_i \hat{H} p_j\rangle$	$-n_i n_j (V_{pp\pi} - V_{pp\sigma})$

and  $H_F$ :

$$H = \begin{pmatrix} H_0 & W \\ W^\dagger & H_F \end{pmatrix}, \quad (2.13)$$

where  $H_0$  and  $H_F$  represent the matrix of the subspaces, and  $W$  and  $W^\dagger$  are the interaction matrices between the two subspaces. Also, a partition of the eigenvector into two eigenvectors of the two subspaces shall be made as:

$$\boldsymbol{\psi} = \begin{pmatrix} \psi_0 \\ \psi_F \end{pmatrix}, \quad (2.14)$$

giving a final eigenvalue equation that depends on the two subspaces with the Löwding partitioning technique as:

$$\begin{pmatrix} H_0 & W \\ W^\dagger & H_F \end{pmatrix} \begin{pmatrix} \psi_0 \\ \psi_F \end{pmatrix} = \varepsilon \begin{pmatrix} \psi_0 \\ \psi_F \end{pmatrix}. \quad (2.15)$$

From Eq. (2.15), we can construct a system of two equations, to find the energy  $\varepsilon$  as a solution

$$H_0\psi_0 + W\psi_F = \varepsilon\psi_0, \quad W^\dagger\psi_0 + H_F\psi_F = \varepsilon\psi_F. \quad (2.16)$$

Solving for  $\psi_F$  from the second equation of Eq. (2.16), we obtain:

$$\psi_F = (\varepsilon - H_F)^{-1} W^\dagger \psi_0, \quad (2.17)$$

and replacing this into the first equation of Eq. (2.16) we get:

$$[H_0 + W(\varepsilon - H_F)^{-1} W^\dagger] \psi_0 = \varepsilon \psi_0. \quad (2.18)$$

This section is supported by [46]. For finding a new effective Hamiltonian  $H_{\text{eff}}$  at low energies, we need to perform an expansion of the term  $(\varepsilon - H_F)^{-1}$  in Eq. (2.18) up to first order in  $\varepsilon$  to obtain  $[H_0 - WH_F^{-1}W^\dagger]\psi_0 \approx \varepsilon S\psi_0$ , where  $S = 1 + WH_F^{-2}W^\dagger$ . Defining  $\Phi = S^{1/2}\psi_0$  and its normalization is given by  $|\Phi|^2 \approx \psi_0^\dagger\psi_0 + \psi_F^\dagger\psi_F$  up to the first order. With this assumptions the equation Eq. (2.18) becomes in:

$$S^{-1/2}[H_0 - WH_F^{-1}W^\dagger]S^{-1/2}\Phi = H_{\text{eff}}\Phi \simeq \varepsilon\Phi. \quad (2.19)$$

Finally, assuming that  $S \approx 1$  the equation Eq. (2.19) becomes into:

$$H_{\text{eff}} \approx H_0 - WH_F^{-1}W^\dagger, \quad (2.20)$$

where  $\langle H_0 \rangle \gg \langle H_F \rangle$ , and  $\langle W \rangle \ll |\langle H_F \rangle - \langle H_0 \rangle|$ . This final equation allow us to find an effective Hamiltonian ( $H_{\text{eff}}$ ) that can be used to add perturbations to the main matrix.



# Chapter 3

## Results and discussion

In this chapter, we develop an analytical tight-binding model for phosphorene. The goal is to explain the main characteristics of its electronic bands around the high symmetry points  $\Gamma$  and S, of the first Brillouin zone defined in Fig. 1.4. We start with a model with a minimum set of orbitals, that in spite of its simplicity, we shall show *a posteriori* that reproduces very well the bands around the mentioned symmetry points. We also explore the influence of other relevant atomic orbitals as a perturbation. In all the cases we compare the bands obtained with our model with the density functional theory bands reported in reference [30].

The importance of choosing the  $\Gamma$  and S points from the first Brillouin zone, remains principally in the mentioned unique characteristics of phosphorene around them, like its anisotropic dispersion and the Rashba splitting around the  $\Gamma$  point, and the intrinsic spin-orbit coupling around the S point [30]. The effects of spin-orbit are however very weak according to DFT calculations, and in any case the role of the spin is beyond to the scope of this dissertation. In spite that we are not going to include the spin, we present our analytical model as a basis to, in the near future, include other interactions like spin-orbit coupling, the stark effect, and magnetism inherited for example from proximity effects.

### 3.1 Tight Binding model for Phosphorene

#### 3.1.1 The basis of $|\phi\rangle$ and $|\theta\rangle$ orbitals

As reported in the literature [30], the DFT bands in phosphorene around the  $\Gamma$  and S points have a strong  $p_z$  character with a small  $p_y$  contribution with a negligible  $p_x$  contribution to the local density of states. Given that we

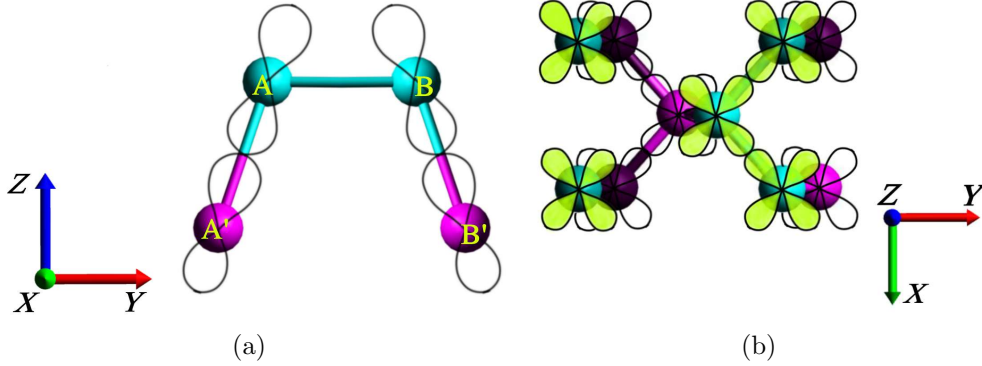


Figure 3.1: The basis of rotated  $|\phi\rangle$  and  $|\theta\rangle$  orbitals in phosphorene. (a) Side view of phosphorene where the  $|\phi\rangle$  orbitals of the four atoms of the basis A', A, B, and B', are represented. These orbitals are slightly rotated in the  $yz$  plane, resulting in a combination of  $p_y$  and  $p_z$  orbitals. (b) Top view of phosphorene picturing the  $|\theta\rangle$  orbitals. These orbitals are rotated in the  $xy$  plane, resulting in a combination of  $p_x$  and  $p_y$  orbitals. The orbitals that are in the top layer atoms are colored in green, and the ones in the bottom layer are colorless. The monolayer of phosphorene lies in the  $xy$  plane.

want to describe the bands around these points, we find convenient for our purposes to choose a basis of tilted atomic orbitals that we shall denote as  $|\phi\rangle$ . These  $|\phi\rangle$  orbitals, extend out of the plane of phosphorene and are not perpendicular to such planes but rotated respect with  $\hat{z}$  and  $\hat{y}$  components, as shown in Fig 3.1a. Explicitly they can be written as:

$$\begin{aligned} |A(A')\phi\rangle &= -n_z |A(A')p_z\rangle - n_y |A(A')p_y\rangle, \\ |B(B')\phi\rangle &= -n_z |B(B')p_z\rangle + n_y |B(B')p_y\rangle, \end{aligned} \quad (3.1)$$

for the atoms labeled as A, A', B and B'. The direction cosines  $n_y$  and  $n_z$  with their respective signs are defined in Eq. (1.2).

In the plane of phosphorene, we can also define a basis of rotated orbitals denoted by  $|\theta\rangle$  (see Fig 3.1b). These orbitals have components  $\hat{x}$  and  $\hat{y}$ , and are given by:

$$\begin{aligned} |A\theta\rangle &= n_{ly} |Ap_y\rangle + n_{lx} |Ap_x\rangle, & |B\theta\rangle &= -n_{ly} |Bp_y\rangle - n_{lx} |Bp_x\rangle, \\ |A'\theta\rangle &= -n_{ly} |A'p_y\rangle + n_{lx} |A'p_x\rangle, & |B'\theta\rangle &= n_{ly} |B'p_y\rangle - n_{lx} |B'p_x\rangle, \end{aligned} \quad (3.2)$$

where the direction cosines  $n_{lx}$  and  $n_{ly}$  are defined in Eq. (1.2).

### 3.1.2 Effective Hamiltonian with $|\phi\rangle$ orbitals

We apply the tight-binding method to calculate the matrix elements defined in Eq. (2.10). We only consider first neighbor interactions between the four atoms of the basis given by  $A - A'$ ,  $A - B$ ,  $B - B'$ , and  $A' - B'$ . So, the coupling matrix elements for  $|\phi\rangle$  orbitals belonging to the same atoms are:

$$\begin{aligned} \langle A\phi|\hat{H}|A\phi\rangle &= (-n_z \langle A p_z| - n_y \langle A p_y|)\hat{H}(-n_z |A p_z\rangle - n_y |A p_y\rangle) \\ &= n_z^2 \langle A p_z|\hat{H}|A p_y\rangle + n_z n_y \langle A p_z|\hat{H}|A p_y\rangle + n_y n_z \langle A p_y|\hat{H}|A p_z\rangle \\ &\quad + n_y^2 \langle A p_y|\hat{H}|A p_y\rangle = \varepsilon_p(n_z^2 + n_y^2) = \varepsilon_p. \end{aligned} \quad (3.3)$$

The procedure to find the other matrix elements for orbitals belonging to the same atom goes in a similar way and are:  $\langle A'\phi|\hat{H}|A'\phi\rangle = \langle B\phi|\hat{H}|B\phi\rangle = \langle B'\phi|\hat{H}|B'\phi\rangle = \varepsilon_p$ .

For  $|\phi\rangle$  orbitals belonging to different atoms, we have:

$$\begin{aligned} \langle A\phi|\hat{H}|B\phi\rangle &= \langle B\phi|\hat{H}|A\phi\rangle = n_z^2 V_{pp\pi} - n_y^2 (n_{ly}^2 V_{pp\sigma} + (1 - n_{ly}^2) V_{pp\pi}) \\ &= V_{AB}, \\ \langle A'\phi|\hat{H}|A\phi\rangle &= \langle A\phi|\hat{H}|A'\phi\rangle = n_z^2 (n_z^2 V_{pp\sigma} + (1 - n_z^2) V_{pp\pi}) \\ &\quad - 2n_y^2 n_z^2 (V_{pp\pi} - V_{pp\sigma}) + n_y^2 (n_y^2 V_{pp\sigma} + (1 - n_y^2) V_{pp\pi}) \\ &= V_{pp\sigma}, \end{aligned} \quad (3.4)$$

where we have used the Slater and Koster parameters defined in Table 2.1. By symmetry:  $\langle A'\phi|\hat{H}|B'\phi\rangle = \langle A\phi|\hat{H}|B\phi\rangle = V_{AB}$ , and  $\langle B'\phi|\hat{H}|B\phi\rangle = \langle A'\phi|\hat{H}|A\phi\rangle = V_{pp\sigma}$ . Finally, the coupling integrals calculated in the basis  $|A\phi\rangle$ ,  $|A'\phi\rangle$ ,  $|B\phi\rangle$ ,  $|B'\phi\rangle$ , are summarized in Table 3.1, where we have taken the reference of energy at  $\varepsilon_p = 0$ .

Table 3.1: Coupling integrals, at first neighbors, between the  $|\phi\rangle$  orbitals of the four atoms of the basis of phosphorene. The reference of energy has been taken at  $\varepsilon_p = 0$ .

	$ A\phi\rangle$	$ A'\phi\rangle$	$ B\phi\rangle$	$ B'\phi\rangle$
$\langle A\phi $	0	$V_{pp\sigma}$	$V_{AB}$	0
$\langle A'\phi $	$V_{pp\sigma}$	0	0	$V_{AB}$
$\langle B\phi $	$V_{AB}$	0	0	$V_{pp\sigma}$
$\langle B'\phi $	0	$V_{AB}$	$V_{pp\sigma}$	0

### 3.1.3 Reciprocal Space Hamiltonian with $|\phi\rangle$ orbitals and band structure

In order to write the Hamiltonian defined by Table 3.1 in the reciprocal space, we proceed by calculating first the diagonal elements and subsequently the non-diagonal elements. By substituting the Bloch function Eq. (2.1) into the transfer integral matrix Eq. (2.10), we obtain the equation for the diagonal AA transfer matrix elements:

$$H_{AA} = \frac{1}{N} \sum_{o=1}^N \sum_{p=1}^N e^{i\mathbf{k}(\mathbf{R}_{A,p}-\mathbf{R}_{A,o})} \langle A\phi(\mathbf{r}-\mathbf{R}_{A,o}) | \hat{H} | A\phi(\mathbf{r}-\mathbf{R}_{A,p}) \rangle. \quad (3.5)$$

The sum in  $o$  goes along all the atoms A of the lattice of phosphorene, but if we consider that the highest contributions come from the interaction of the atom with itself  $o = p$  (onsite energies), we have that  $\langle A\phi(\mathbf{r}-\mathbf{R}_{A,o}) | \hat{H} | A\phi(\mathbf{r}-\mathbf{R}_{A,p}) \rangle = \langle A\phi(\mathbf{r}-\mathbf{R}_{A,o}) | \hat{H} | A\phi(\mathbf{r}-\mathbf{R}_{A,o}) \rangle = 0$ , because we have defined our reference at  $\varepsilon_p = 0$ . The same applies to the other diagonal elements corresponding to the other atoms of the basis.

For the off-diagonal matrix elements we have the equation:

$$H_{AB} = \frac{1}{N} \sum_{o=1}^N \sum_{p=1}^N e^{i\mathbf{k}(\mathbf{R}_{B,p}-\mathbf{R}_{A,o})} \langle A\phi(\mathbf{r}-\mathbf{R}_{A,o}) | \hat{H} | B\phi(\mathbf{r}-\mathbf{R}_{B,p}) \rangle, \quad (3.6)$$

where the sum in  $p$  runs over all the atoms B of the lattice. If we consider that the highest contribution in the sum comes from the interaction between an atom A and its two first neighbors B, then:

$$H_{AB} \approx \frac{1}{N} \sum_{o=1}^N \sum_{l=1}^2 e^{i\mathbf{k}\cdot\boldsymbol{\delta}_{ABl}} \langle A\phi(\mathbf{r}-\mathbf{R}_{A,o}) | \hat{H} | B\phi(\mathbf{r}-\mathbf{R}_{B,l}) \rangle, \quad (3.7)$$

where  $\boldsymbol{\delta}_{ABl}$  is the A – B distance defined in Eq. (1.2). The coupling between A and its first neighbors B is defined in Table 3.1, and is independent of the index  $l$ , therefore:

$$H_{AB} \approx \frac{1}{N} \sum_{o=1}^N \sum_{l=1}^2 e^{i\mathbf{k}\cdot\boldsymbol{\delta}_{ABl}} V_{AB} = V_{AB} \sum_{l=1}^2 e^{i\mathbf{k}\cdot\boldsymbol{\delta}_{ABl}} = V_{AB} f(\mathbf{k}), \quad (3.8)$$

where  $V_{AB}$  is extracted from Table 3.1 and defined in equation Eq. (3.4), and we have defined the form factor:

$$f(\mathbf{k}) = \sum_{l=1}^2 e^{i\mathbf{k}\cdot\boldsymbol{\delta}_{ABl}} = 2e^{ik_y y} \cos\left(\frac{bk_x}{2}\right), \quad (3.9)$$

where  $\mathbf{k} = k_x \hat{x} + k_y \hat{y}$  represents the wave vector in the 2D plane. With a similar procedure, we obtain that the rest of the off-diagonal elements are given by:

$$\begin{aligned} H_{A'B'} &= \sum_l e^{i\mathbf{k} \cdot \boldsymbol{\delta}_{A'B'_l}} \langle A' \phi | \hat{H} | B'_l \phi \rangle = V_{AB} f(\mathbf{k}) \\ H_{AA'} &= e^{i\mathbf{k} \cdot \boldsymbol{\delta}_{AA'}} \langle A \phi | \hat{H} | A' \phi \rangle = V_{pp\sigma} g(\mathbf{k}), \\ H_{BB'} &= e^{i\mathbf{k} \cdot \boldsymbol{\delta}_{BB'}} \langle B \phi | \hat{H} | B' \phi \rangle = V_{pp\sigma} g^*(\mathbf{k}), \end{aligned} \quad (3.10)$$

where;  $\boldsymbol{\delta}_{AA'}$ ,  $\boldsymbol{\delta}_{BB'}$ , and  $\boldsymbol{\delta}_{A'B'_l}$  are defined in Eq. (1.2); the letters  $h = b_2 \sin \phi$ ,  $y = b_1 \cos \theta$ , and  $b = 2b_1 \sin \theta$ , respectively, and  $g(\mathbf{k}) = e^{-ik_y h}$ . With all these elements, the  $4 \times 4$  Hamiltonian in the reciprocal space, in the basis  $|A\phi\rangle$ ,  $|A'\phi\rangle$ ,  $|B\phi\rangle$ ,  $|B'\phi\rangle$ , is:

$$H^\phi(\mathbf{k}) = \begin{pmatrix} 0 & V_{pp\sigma} g(\mathbf{k}) & V_{AB} f(\mathbf{k}) & 0 \\ V_{pp\sigma} g^*(\mathbf{k}) & 0 & 0 & V_{AB} f^*(\mathbf{k}) \\ V_{AB} f^*(\mathbf{k}) & 0 & 0 & V_{pp\sigma} g^*(\mathbf{k}) \\ 0 & V_{AB} f(\mathbf{k}) & V_{pp\sigma} g(\mathbf{k}) & 0 \end{pmatrix}. \quad (3.11)$$

From the Hamiltonian of Eq. (3.11) we calculated the eigenvalues around the  $\Gamma$  point, in the directions in  $\Gamma - X$  and  $\Gamma - Y$ :

$$\begin{aligned} \varepsilon_{\Gamma X}(\pm) &= (\pm) \sqrt{2V_{AB}^2 + V_{pp\sigma}^2 - 4\sqrt{V_{AB}^2 V_{pp\sigma}^2 \cos^2[bk_x/2] + 2V_{AB}^2 \cos[bk_x]}}, \\ \varepsilon_{\Gamma X}(\pm) &= (\pm) \sqrt{2V_{AB}^2 + V_{pp\sigma}^2 + 4\sqrt{V_{AB}^2 V_{pp\sigma}^2 \cos^2[bk_x/2] + 2V_{AB}^2 \cos[bk_x]}}, \\ \varepsilon_{\Gamma Y}(\pm) &= (\pm) e^{-ik_y(h+y)} \sqrt{-2\sqrt{(e^{ik_y(h+y)} + e^{3ik_y(h+y)})^2 V_{AB}^2 V_{pp\sigma}^2 + e^{2ik_y(h+y)}(4V_{AB}^2 + V_{pp\sigma}^2)}, \\ \varepsilon_{\Gamma Y}(\pm) &= (\pm) e^{-ik_y(h+y)} \sqrt{2\sqrt{(e^{ik_y(h+y)} + e^{3ik_y(h+y)})^2 V_{AB}^2 V_{pp\sigma}^2 + e^{2ik_y(h+y)}(4V_{AB}^2 + V_{pp\sigma}^2)}, \end{aligned} \quad (3.12)$$

and expanding up to quadratic order the bands that open the gap, which are the first and third equations from Eq. (3.12), we obtain (A calculation of the continuum Hamiltonian around the  $\Gamma$  point is shown in Appendix A.):

$$\varepsilon_{\Gamma X}(\pm) = (\pm)(\alpha + \beta k_x^2), \quad \varepsilon_{\Gamma Y}(\pm) = (\pm)(\alpha + \gamma k_y^2), \quad (3.13)$$

where  $\varepsilon_{\Gamma X}$  and  $\varepsilon_{\Gamma Y}$  represent the eigenvalues in the  $\Gamma - X$  and  $\Gamma - Y$  directions, and the (+) and (-) represent the conduction and the valence bands

respectively, and the constants  $\alpha$ ,  $\beta$ , and  $\gamma$  are:

$$\begin{aligned}\alpha &= \sqrt{4V_{\text{AB}}^2 + V_{pp\sigma}^2 - 4\sqrt{V_{\text{AB}}^2 V_{pp\sigma}^2}}, \\ \beta &= \frac{b^2 \left( -2V_{\text{AB}}^2 + \sqrt{V_{\text{AB}}^2 V_{pp\sigma}^2} \right)}{4\sqrt{4V_{\text{AB}}^2 + V_{pp\sigma}^2 - 4\sqrt{V_{\text{AB}}^2 V_{pp\sigma}^2}}}, \\ \gamma &= \frac{\sqrt{V_{\text{AB}}^2 V_{pp\sigma}^2} (h + y)^2}{\sqrt{4V_{\text{AB}}^2 + V_{pp\sigma}^2 - 4\sqrt{V_{\text{AB}}^2 V_{pp\sigma}^2}}}.\end{aligned}\tag{3.14}$$

Table 3.2: Table with the Slater and Koster parameters obtained from the fitting with the DFT bands from [30], for the model of  $|\phi\rangle$  orbitals.  $V_{pp\sigma}$  and  $V_{pp\pi}$  are the SK parameters for hopping between  $p_z$  and  $p_y$  orbitals forming  $\sigma$  and  $\pi$  bonds respectively.  $V_{\text{AB}}$  is the hopping parameter between A(A') and B(B') atoms (see Eq. 3.4).

Parameter	Value (eV)	Values of Ref. [32] (eV)
$V_{pp\sigma}$	3.042	4.03
$V_{pp\pi}$	-1.002	-1.14
$V_{\text{AB}}$	-0.971	-

Table 3.3: Table with numerical values of  $\alpha$ ,  $\beta$ , and  $\gamma$  expressed in Eq. (3.14). These values were obtained from the tight-binding parameters from Table. 3.2.

Parameter	Value
$\alpha$ (eV)	1.09
$\beta$ (eV nm <sup>2</sup> )	0.027
$\gamma$ (eV nm <sup>2</sup> )	0.14

The effective masses along the  $\Gamma - X$  and  $\Gamma - Y$  directions are obtained from  $1/m_{ij}^* = (1/\hbar^2)(\partial^2\varepsilon/\partial k_i\partial k_j)$  and are given by:

$$m_{\Gamma X}^*(\pm) = (\pm)\frac{\hbar^2}{2\beta}, \quad m_{\Gamma Y}^*(\pm) = (\pm)\frac{\hbar^2}{2\gamma},\tag{3.15}$$

Table 3.4: Table with numerical values of the effective masses in  $\Gamma - X$  and  $\Gamma - Y$  directions calculated from Eq. (3.15) and compared with reference [36]. Our values has been normalized by the rest mass of the electron.

Effective mass $m^*$	Our values	Values from Ref. [36]
Conduction $m_{\Gamma X}^*$	1.40	1.15
Conduction $m_{\Gamma Y}^*$	0.27	0.24
Valence $m_{\Gamma X}^*$	1.40	7.29
Valence $m_{\Gamma Y}^*$	0.27	0.24

where  $i = j = x$  in the  $\Gamma - X$  direction and  $i = j = y$  in the  $\Gamma - Y$  direction.

The effective mass values obtained from our model are compared with the effective mass values of Ref. [36] and are shown in Table 3.4. As can be seen in this table, our values of effective masses are equal for the conduction and valence band given a direction ( $\Gamma - X$  or  $\Gamma - Y$ ), but they are different for a given band (conduction or valence) in the direction  $\Gamma - X$  and  $\Gamma - Y$ . The values reported in reference [36], however, have a numerical difference for the conduction and valence band in the  $\Gamma - X$  direction, which can not be reproduced by our model. This is because our effective mass values have been calculated from Eq. (3.13), where the eigenvalues for the same direction differ only in sign.

When analyzing the dependence of the effective masses in both directions in Eq. (3.15) and the constants defined in Eq. (3.14), we can see that the difference between the constants  $\beta$  and  $\gamma$  is the term  $-2V_{AB}^2$ , that appears in the numerator of  $\beta$ , and the multiplicative geometrical parameters  $b^2/4 = 2.81\text{\AA}^2$  in  $\beta$  and  $(h + y)^2 = 5.37\text{\AA}^2$  in  $\gamma$ . These geometrical parameters differ by a factor of approximately 2, however,  $\beta$  is about one order of magnitude smaller than  $\gamma$  (see Table.3.3). Therefore, we can conclude that what makes the effective masses so different in the  $\Gamma - X$  and the  $\Gamma - Y$  directions is the term  $-2V_{AB}^2$  in  $\beta$ . In this term,  $V_{AB}$  is the hopping parameter between A and B atoms, given by a combination of the Slater and Koster parameters  $V_{pp\sigma}$  and  $V_{pp\pi}$  (see Eq. 3.4).

At the S point, the S- $\Gamma$  direction is defined by substituting  $k_x = (\pi/b) + k_s$  and  $k_y = (\pi/a) + k_s$  in Eq. (3.11), where  $k_s$  is the wavenumber around the point S. The respective eigenvalues obtained directly from the Eq. (3.11) are:

$$\varepsilon_{S\Gamma, v(c)\pm} = -(+) \left( (2V_{AB}^2 + V_{pp\sigma}^2 - 2V_{AB}^2 \cos(bk_s)) \pm (\mp) 4V_{AB}V_{pp\sigma} \sin\left(\frac{bk_s}{2}\right) \sin\left(\frac{ak_s}{2}\right) \right)^{1/2}, \quad (3.16)$$

where the letter  $v$  corresponds to the valence band and  $c$  to the conduction band. The signs  $+$  and  $-$  are related to the positive and negative effective masses respectively.

In the  $S-X$  direction, we use  $k_x = (\pi/b) + k_s$  and  $k_y = (\pi/a)$  in Eq. (3.11). The eigenvalues obtained from Eq. (3.11) are:

$$\varepsilon_{\text{SX},v(c)\pm} = -(+)(2V_{\text{AB}}^2 + V_{pp\sigma}^2 - 2V_{\text{AB}}^2 \cos(bk_s)). \quad (3.17)$$

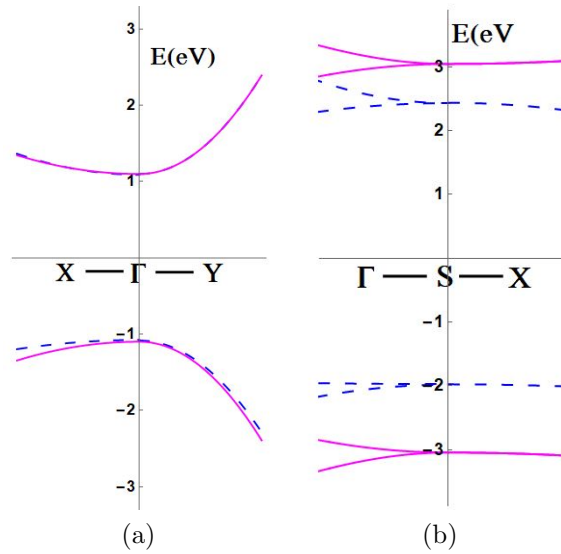


Figure 3.2: Electronic band structure of phosphorene. (a) Valence and conduction bands around the  $\Gamma$  point in the  $\Gamma-X$  and  $\Gamma-Y$  directions. (b) Valence and conduction bands around the  $S$  point in the  $S-\Gamma$  and  $S-X$  directions. In both cases, the blue (-dashed-) lines are quadratic fits of the DFT bands taken from [30], and the magenta (solid) lines are the eigenvalues from Eqs. (3.13), (3.16), and (3.17), given by our tight-binding model with  $|\phi\rangle$  orbitals from Eq. (3.11).

The bands calculated with our tight-binding model (Eqs. (3.13), (3.16), and (3.17)), are plotted in Fig. 3.2 and represented by magenta (solid) lines. The values of the Slater and Koster parameters, obtained from the fitting to the DFT bands (blue (-dashed-) lines), are given in Table 3.2. In Fig. 3.2, the DFT bands used to compare with our tight-binding model were obtained by taking data points from the band structure of reference [30] (Fig. 1.4), around the  $\Gamma$  and  $S$  points. These data points were extracted and fitted



to quadratic functions that reproduce the DFT bands around the  $\Gamma$  and S points, in each direction  $X - \Gamma - Y$  and  $\Gamma - S - X$ .

As we can see in Fig. 3.2a, our model fits very well the highest valence and lower conduction bands compared with the DFT model around the  $\Gamma$  point. The more relevant features of the bands, like the difference between the effective masses in the  $\Gamma - X$  and  $\Gamma - Y$  directions, are reproduced. Also, we find a bandgap of 2.19 eV, which is very close to the one obtained by DFT (2.17 eV). One characteristic we were not able to reproduce with our model of  $|\phi\rangle$  orbitals, is a slight difference between the effective masses of the valence and conduction DFT bands in a direction ( $\Gamma - X$ ). On the other hand, around the S point Fig. 3.2b, our model reproduces very well the shape of the bands (compared to the DFT), but it can not reproduce the correct band-gap between them. Finally, in all the cases, we compared the Slater and Koster parameters obtained with our model with the ones reported by Menezes *et. al.* (Table 1 in reference [32]), finding that they are in very close agreement.

In the next section, we will evaluate if the addition of other orbitals in order to figure out if this refined model can improve the discrepancies observed between our model with only  $|\phi\rangle$  orbitals and the DFT bands used as of reference [30].

### 3.1.4 Effective Hamiltonian with $|\phi\rangle$ orbitals perturbed by $|\theta\rangle$ orbitals, and band structure

To include perturbatively the  $|\theta\rangle$  orbitals described in Section 3.1.1 and given by Eq. (3.2), we use the technique of Löwding transformation. Before this, we calculate the matrix elements (Eq. (2.10)), considering only interaction between first neighbors. For  $|\theta\rangle$  orbitals belonging to the same atoms we have:

$$\begin{aligned} \langle A\theta|\hat{H}|A\theta\rangle &= (n_{ly}\langle Ap_y| + n_{lx}\langle Ap_x|)\hat{H}(n_{ly}|Ap_y\rangle + n_{lx}|Ap_x\rangle) \\ &= n_{ly}^2\langle Ap_y|\hat{H}|Ap_y\rangle + n_{ly}n_{lx}\langle Ap_y|\hat{H}|Ap_x\rangle + n_{lx}n_{ly}\langle Ap_x|\hat{H}|Ap_y\rangle \\ &\quad + n_{lx}^2\langle Ap_x|\hat{H}|Ap_x\rangle = \varepsilon_p. \end{aligned} \tag{3.18}$$

The procedure to find the other matrix elements of the same kind goes in a similar way and are:  $\langle A'\theta|\hat{H}|A'\theta\rangle = \langle B\theta|\hat{H}|B\theta\rangle = \langle B'\theta|\hat{H}|B'\theta\rangle = \varepsilon_p$ .

The hopping integrals for  $|\theta\rangle$  orbitals belonging to different atoms are:

$$\begin{aligned}
\langle A\theta|\hat{H}|B\theta\rangle &= \langle B\theta|\hat{H}|A\theta\rangle = -n_{ly}^2(n_{lx}^2V_{pp\sigma} + (1 - n_{ly}^2)V_{pp\pi}) \\
&\quad + 2n_{ly}^2n_{lx}^2(V_{pp\pi} - V_{pp\sigma}) - n_{lx}^2(n_{ly}^2V_{pp\sigma} + (1 - n_{lx}^2)V_{pp\pi}) \\
&= -V_{pp\sigma}, \\
\langle A'\theta|\hat{H}|A\theta\rangle &= \langle A\theta|\hat{H}|A'\theta\rangle = n_{lx}^2V_{pp\pi} - n_{ly}^2(n_{lx}^2V_{pp\sigma} + (1 - n_{ly}^2)V_{pp\pi}) \\
&= V_{AA},
\end{aligned} \tag{3.19}$$

where we have used the Slater and Koster parameters defined in Table 2.1. By symmetry:  $\langle A'\theta|\hat{H}|B'\theta\rangle = \langle A\theta|\hat{H}|B\theta\rangle = -V_{pp\sigma}$ , and  $\langle B'\theta|\hat{H}|B\theta\rangle = \langle A'\theta|\hat{H}|A\theta\rangle = V_{AA}$ . Finally, the hopping and onsite integrals, calculated in the basis  $|A\theta\rangle$ ,  $|A'\theta\rangle$ ,  $|B\theta\rangle$ ,  $|B'\theta\rangle$ , are summarized in Table 3.5, where we have taken the reference of energy at  $\varepsilon_p = 0$ . The matrix elements for the

Table 3.5: Hopping and onsite integrals, at first neighbors, between the  $|\theta\rangle$  orbitals of the four atoms of the basis of phosphorene. The reference of energy has been taken at  $\varepsilon_p = 0$ .

	$ A\theta\rangle$	$ A'\theta\rangle$	$ B\theta\rangle$	$ B'\theta\rangle$
$\langle A\theta $	0	$V_{AA}$	$-V_{pp\sigma}$	0
$\langle A'\theta $	$V_{AA}$	0	0	$-V_{pp\sigma}$
$\langle B\theta $	$-V_{pp\sigma}$	0	0	$V_{AA}$
$\langle B'\theta $	0	$-V_{pp\sigma}$	$V_{AA}$	0

hopping between  $|\phi\rangle$  and  $|\theta\rangle$  orbitals belonging to the same atom are:

$$\begin{aligned}
\langle A\phi|\hat{H}|A\theta\rangle &= (-n_z \langle A p_z| - n_y \langle A p_y|) \hat{H} (n_{ly} |A p_y\rangle + n_{lx} |A p_x\rangle) \\
&= -n_z n_{ly} \langle A p_z|\hat{H}|A p_y\rangle - n_z n_{lx} \langle A p_z|\hat{H}|A p_x\rangle \\
&\quad - n_y n_{ly} \langle A p_y|\hat{H}|A p_y\rangle - n_y n_{lx} \langle A p_y|\hat{H}|A p_x\rangle = -n_y n_{ly} \varepsilon_p.
\end{aligned} \tag{3.20}$$

In the same way, the other matrix elements are:  $\langle A'\phi|\hat{H}|A'\theta\rangle = \langle B\phi|\hat{H}|B\theta\rangle = \langle B'\phi|\hat{H}|B'\theta\rangle = -n_y n_{ly} \varepsilon_p$ .

The hopping integrals for  $|\phi\rangle$  and  $|\theta\rangle$  orbitals from different atoms, are:

$$\begin{aligned}
\langle A\phi|\hat{H}|B\theta\rangle &= \langle B\theta|\hat{H}|A\phi\rangle = n_z n_{ly}(-n_{lz} n_{ly}(V_{pp\pi} - V_{pp\sigma})) \\
&\quad + n_z n_{lx}(-n_{lz} n_{lx}(V_{pp\pi} - V_{pp\sigma})) + n_y n_{ly}(n_{ly}^2 V_{pp\sigma} + (1 - n_{ly}^2 V_{pp\pi})) \\
&\quad + n_y n_{lx}(-n_{ly} n_{lx}(V_{pp\pi} - V_{pp\sigma})) = n_y n_{ly} V_{pp\sigma}, \\
\langle A'\phi|\hat{H}|B'\theta\rangle &= \langle B'\theta|\hat{H}|A'\phi\rangle = -n_z n_{ly}(n_{lz} n_{ly}(V_{pp\pi} - V_{pp\sigma})) \\
&\quad + n_z n_{lx}(n_{lz} n_{lx}(V_{pp\pi} - V_{pp\sigma})) - n_y n_{ly}(n_{ly}^2 V_{pp\sigma} + (1 - n_{ly}^2 V_{pp\pi})) \\
&\quad + n_y n_{lx}(n_{ly} n_{lx}(V_{pp\pi} - V_{pp\sigma})) = -n_y n_{ly} V_{pp\sigma}, \\
\langle A\phi|\hat{H}|A'\theta\rangle &= \langle A'\theta|\hat{H}|A\phi\rangle = n_z n_{ly}(-n_z n_y(V_{pp\pi} - V_{pp\sigma})) \\
&\quad - n_z n_{lx}(-n_z n_x(V_{pp\pi} - V_{pp\sigma})) + n_y n_{ly}(n_{ly}^2 V_{pp\sigma} + (1 - n_{ly}^2 V_{pp\pi})) \\
&\quad - n_y n_{lx}(-n_y n_x(V_{pp\pi} - V_{pp\sigma})) = n_y n_{ly} V_{pp\sigma},
\end{aligned} \tag{3.21}$$

where we have used the Slater and Koster parameters defined in Table 2.1. By symmetry:  $\langle B\phi|\hat{H}|B'\theta\rangle = \langle A\phi|\hat{H}|A'\theta\rangle = n_y n_{ly} V_{pp\sigma}$ . Finally, the hopping and onsite integrals between  $|\phi\rangle$  and  $|\theta\rangle$  orbitals, are summarized in Table 3.6, where we have taken the reference of energy at  $\varepsilon_p = 0$ .

Table 3.6: Overlap integrals, at first neighbors, between the  $|\phi\rangle$  and  $|\theta\rangle$  orbitals of the four atoms of the basis of phosphorene. The reference of energy has been taken at  $\varepsilon_p = 0$ .

	$ A\theta\rangle$	$ A'\theta\rangle$	$ B\theta\rangle$	$ B'\theta\rangle$
$\langle A\phi $	0	$n_y n_{ly} V_{pp\sigma}$	$n_y n_{ly} V_{pp\sigma}$	0
$\langle A'\phi $	$-n_y n_{ly} V_{pp\sigma}$	0	0	$-n_y n_{ly} V_{pp\sigma}$
$\langle B\phi $	$n_y n_{ly} V_{pp\sigma}$	0	0	$n_y n_{ly} V_{pp\sigma}$
$\langle B'\phi $	0	$-n_y n_{ly} V_{pp\sigma}$	$-n_y n_{ly} V_{pp\sigma}$	0

Now we apply the Löwding transformation method given by Eq. (2.20), where the four sub-matrices are taken as follows:  $H_0$  is the real space Hamiltonian matrix for  $|\phi\rangle$  orbitals (Table 3.1),  $H_F$  is the real space Hamiltonian matrix for  $|\theta\rangle$  orbitals (Table 3.5),  $W$  is the overlap matrix between  $|\phi\rangle$  and  $|\theta\rangle$  (Table 3.6), and  $W^\dagger$  is the conjugated matrix of  $W$ . Once, these elements are ready, we write the real space effective Hamiltonian for  $|\phi\rangle$  orbitals per-

turbed by  $|\theta\rangle$  as:

$$H_{\text{eff}}^{\theta} \approx H_0 - WH_F^{-1}W^{\dagger} \approx \begin{pmatrix} 0 & V_{pp\sigma}^{\theta} & V_{AB}^{\theta} & 0 \\ V_{pp\sigma}^{\theta} & 0 & 0 & V_{AB}^{\theta} \\ V_{AB}^{\theta} & 0 & 0 & V_{pp\sigma}^{\theta} \\ 0 & V_{AB}^{\theta} & V_{pp\sigma}^{\theta} & 0 \end{pmatrix}, \quad (3.22)$$

where the super index  $\theta$  represents the perturbation with  $|\theta\rangle$  orbitals, and the matrix elements are:

$$V_{pp\sigma}^{\theta} = V_{pp\sigma} + \frac{(2n_{ly}^2 n_y^2 V_{pp\sigma}^2)}{(V_{AA} - V_{pp\sigma})}, \quad V_{AB}^{\theta} = V_{AB} - \frac{(2n_{ly}^2 n_y^2 V_{pp\sigma}^2)}{(V_{AA} - V_{pp\sigma})}. \quad (3.23)$$

The Hamiltonian in the reciprocal space, considering the nearest first neighbors contributions, can be calculated with a procedure similar to the one shown in Subsec. 3.1.3 (Eqs. (3.5) to (3.10) ), and is given by:

$$H^{\theta}(\mathbf{k}) = \begin{pmatrix} 0 & V_{pp\sigma}^{\theta}g(\mathbf{k}) & V_{AB}^{\theta}f(\mathbf{k}) & 0 \\ V_{pp\sigma}^{\theta}g^*(\mathbf{k}) & 0 & 0 & V_{AB}^{\theta}f^*(\mathbf{k}) \\ V_{AB}^{\theta}f^*(\mathbf{k}) & 0 & 0 & V_{pp\sigma}^{\theta}g^*(\mathbf{k}) \\ 0 & V_{AB}^{\theta}f(\mathbf{k}) & V_{pp\sigma}^{\theta}g(\mathbf{k}) & 0 \end{pmatrix}. \quad (3.24)$$

From the Hamiltonian of Eq. (3.24), we obtain the eigenvalues around the high symmetry points  $\Gamma$  and S of the first Brillouin zone. All the calculations mentioned before are similar to those for  $|\phi\rangle$  orbitals without perturbation (see Eqs. (3.13), (3.16), and (3.17)), the only difference is the change in the parameters  $V_{pp\sigma}$  and  $V_{AB}$  by  $V_{pp\sigma}^{\theta}$  and  $V_{AB}^{\theta}$  (see Eq. (3.23)).

Table 3.7: Table with the Slater and Koster parameters obtained from the fitting with the DFT bands, for the model of  $|\phi\rangle$  perturbed by  $|\theta\rangle$  orbitals. Where  $V_{pp\sigma}$  and  $V_{pp\pi}$  are the SK parameters for the hopping between  $p$  orbitals forming  $\sigma$  or  $\pi$  bonds.  $V_{AB}$  is the hopping parameter between  $|\phi\rangle$  orbitals of the A(A') and B(B') atoms (see Eq. (3.4)), and  $V_{AA}$  is the hopping parameter between  $|\theta\rangle$  orbitals of the A(B) and A'(B'), atoms (see Eq. (3.19)).

Parameter	Value (eV)	Values of Ref. [32] (eV)
$V_{pp\sigma}$	3.22	4.03
$V_{pp\pi}$	-5	-1.14
$V_{AB}$	-1.2	-
$V_{AA}$	-1.09	-

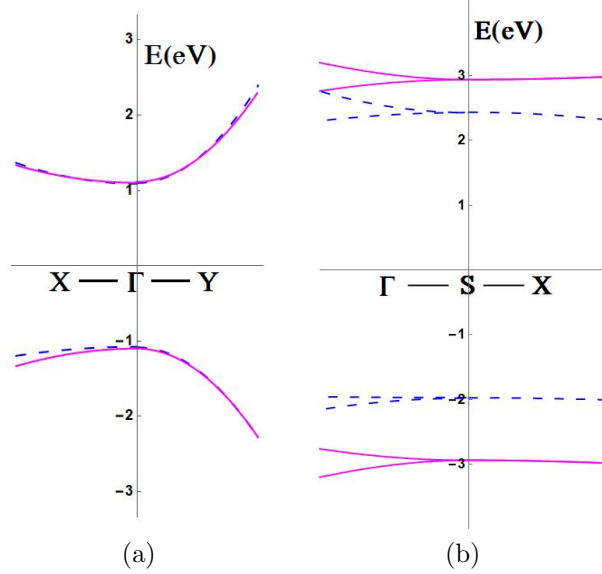


Figure 3.3: Band structure of phosphorene with  $|\phi\rangle$  orbitals perturbed by  $|\theta\rangle$  orbitals. (a) Valence and conduction bands around  $\Gamma$  point in the  $X-\Gamma-Y$  directions. (b) Valence and conduction bands around the  $S$  point in the  $\Gamma-S-X$  directions. In both cases, the blue (-dashed-) lines represent the DFT fitting taken from [30], and the magenta (solid) lines represent the eigenvalues obtained by our tight-binding model from Eq. (3.24).

The electronic band structure of phosphorene in the vicinity of the  $\Gamma$  and  $S$  points is shown in Fig. 3.3 and was adjusted by the SK parameters from the Table. 3.7. As we can see in Fig. 3.3a, our model (magenta (solid) lines), reproduce again the asymmetry of the bands around the  $\Gamma$  point in comparison with the DFT model (blue (-dashed-) lines), with a band-gap of 2.31 eV that is still close to the one obtained by DFT 2.17 eV. On the other hand, around the  $S$  point, the change that we can see, compared with the model of only  $|\phi\rangle$  orbitals, is that the bands are closer in energy to those given by DFT. Finally, we compared the Slater and Koster parameters obtained with our model with the ones reported by Menezes *et. al.* (Table 1 in reference [32]), finding that they are in the same order of magnitude.

### 3.1.5 Effective Hamiltonian with $|\phi\rangle$ orbitals perturbed by $s$ orbitals, and band structure

In order to include perturbatively the  $s$  orbitals, we proceed as we did in Section 3.1.1, first we find the hopping integrals between the same atoms

(on-site), using the Slater-Koster parameters from Table 2.1 in Sec. 2, and considering only the interaction between the first neighbors. Following this we have:

$$\langle \text{As} | \hat{H} | \text{As} \rangle = \langle \text{Bs} | \hat{H} | \text{Bs} \rangle = \langle \text{A's} | \hat{H} | \text{A's} \rangle = \langle \text{B's} | \hat{H} | \text{B's} \rangle = \varepsilon_s, \quad (3.25)$$

where  $\varepsilon_s$  is the on-site energy for the  $s$  orbitals. For  $s$  orbitals belonging to different atoms, we have:

$$\langle \text{As} | \hat{H} | \text{Bs} \rangle = \langle \text{A's} | \hat{H} | \text{B's} \rangle = \langle \text{As} | \hat{H} | \text{A's} \rangle = \langle \text{B's} | \hat{H} | \text{Bs} \rangle = V_{ss\sigma}. \quad (3.26)$$

The Slater and Koster integrals calculated with a basis of  $|\text{As}\rangle$ ,  $|\text{A's}\rangle$ ,  $|\text{Bs}\rangle$ ,  $|\text{B's}\rangle$  are indicated in Table 3.8.

Table 3.8: Hopping and onsite integrals, at first neighbors, between the  $s$  orbitals of the four atoms of the basis of phosphorene.

	$ \text{As}\rangle$	$ \text{A's}\rangle$	$ \text{Bs}\rangle$	$ \text{B's}\rangle$
$\langle \text{As}  $	$\varepsilon_s$	$V_{ss\sigma}$	$V_{ss\sigma}$	0
$\langle \text{A's}  $	$V_{ss\sigma}$	$\varepsilon_s$	0	$V_{ss\sigma}$
$\langle \text{Bs}  $	$V_{ss\sigma}$	0	$\varepsilon_s$	$V_{ss\sigma}$
$\langle \text{B's}  $	0	$V_{ss\sigma}$	$V_{ss\sigma}$	$\varepsilon_s$

The hopping integrals between the orbitals  $|\phi\rangle$  and  $|s\rangle$  belonging to the same atoms are:

$$\begin{aligned} \langle \text{A}\phi | \hat{H} | \text{As} \rangle &= \langle \text{As} | \hat{H} | \text{A}\phi \rangle = (-n_z \langle \text{Ap}_z | - n_y \langle \text{Ap}_y |) \hat{H} | \text{As} \rangle = -n_z \langle \text{Ap}_z | \hat{H} | \text{As} \rangle \\ &\quad - n_y \langle \text{Ap}_y | \hat{H} | \text{As} \rangle = 0, \end{aligned} \quad (3.27)$$

and in the case for the other atoms, the result goes in the same way, as:  $\langle \text{B}\phi | \hat{H} | \text{Bs} \rangle = \langle \text{A's}\phi | \hat{H} | \text{A's} \rangle = \langle \text{B's}\phi | \hat{H} | \text{B's} \rangle = 0$ . The hopping integrals between the orbitals  $|\phi\rangle$  and  $|s\rangle$  belonging to different atoms are given by:

$$\begin{aligned} \langle \text{A}\phi | \hat{H} | \text{Bs} \rangle &= \langle \text{Bs} | \hat{H} | \text{A}\phi \rangle = (-n_z \langle \text{Ap}_z | - n_y \langle \text{Ap}_y |) \hat{H} | \text{Bs} \rangle = -n_z \langle \text{Ap}_z | \hat{H} | \text{Bs} \rangle \\ &\quad - n_y \langle \text{Ap}_y | \hat{H} | \text{Bs} \rangle = n_z n_{lz} V_{sp\sigma} + n_y n_{ly} V_{sp\sigma} = n_y n_{ly} V_{sp\sigma}, \\ \langle \text{B}\phi | \hat{H} | \text{As} \rangle &= \langle \text{As} | \hat{H} | \text{B}\phi \rangle = -n_y n_{ly} V_{sp\sigma}, \\ \langle \text{A}\phi | \hat{H} | \text{A's} \rangle &= \langle \text{A's} | \hat{H} | \text{A}\phi \rangle = (-n_z \langle \text{Ap}_z | - n_y \langle \text{Ap}_y |) \hat{H} | \text{A's} \rangle = -n_z \langle \text{Ap}_z | \hat{H} | \text{A's} \rangle \\ &\quad - n_y \langle \text{Ap}_y | \hat{H} | \text{A's} \rangle = -n_z n_z V_{sp\sigma} - n_y n_y V_{sp\sigma} = -V_{sp\sigma}, \\ \langle \text{A's}\phi | \hat{H} | \text{As} \rangle &= \langle \text{As} | \hat{H} | \text{A's}\phi \rangle = -n_z n_z V_{sp\sigma} + n_y n_y V_{sp\sigma} = V_{sp\sigma}, \end{aligned} \quad (3.28)$$

where we have used the Slater and Koster parameters defined in Table 2.1. By symmetry:  $\langle B'\phi|\hat{H}|A's\rangle = \langle A\phi|\hat{H}|Bs\rangle = n_y n_{ly} V_{sp\sigma}$ ,  $\langle A'\phi|\hat{H}|B's\rangle = \langle B'\phi|\hat{H}|A's\rangle = -n_y n_{ly} V_{sp\sigma}$ ,  $\langle B\phi|\hat{H}|B's\rangle = \langle A\phi|\hat{H}|A's\rangle = -V_{sp\sigma}$ ,  $\langle B'\phi|\hat{H}|Bs\rangle = \langle A'\phi|\hat{H}|As\rangle = V_{sp\sigma}$ . Finally, the transfer integral matrix between  $|\phi\rangle$  and  $s$  orbitals is summarized in Table 3.9.

Table 3.9: Transfer integral matrix, at first neighbors, between the  $|\phi\rangle$  and  $s$  orbitals of the four atoms of the basis of phosphorene. The reference of energy has been taken at  $\varepsilon_p = 0$ .

	$ As\rangle$	$ A's\rangle$	$ Bs\rangle$	$ B's\rangle$
$\langle A\phi $	0	$-V_{sp\sigma}$	$n_y n_{ly} V_{sp\sigma}$	0
$\langle A'\phi $	$V_{sp\sigma}$	0	0	$-n_y n_{ly} V_{sp\sigma}$
$\langle B\phi $	$-n_y n_{ly} V_{sp\sigma}$	0	0	$-V_{sp\sigma}$
$\langle B'\phi $	0	$n_y n_{ly} V_{sp\sigma}$	$V_{sp\sigma}$	0

Now, we apply the Löwding transformation method given by Eq. (2.20) where the four sub-matrices are taken as follows:  $H_0$  is the real space Hamiltonian matrix for  $|\phi\rangle$  orbitals (Table 3.1),  $H_F$  is the real space Hamiltonian matrix for  $s$  orbitals (Table 3.8),  $W$  is the overlap matrix between  $|\phi\rangle$  and  $s$  (Table 3.9), and  $W^\dagger$  is the conjugated matrix of  $W$ . Once, these elements are ready, we write the real space effective Hamiltonian for  $|\phi\rangle$  orbitals perturbed by  $s$  as:

$$H_{\text{eff}}^s \approx \begin{pmatrix} \varepsilon_{s1} & V_{pp\sigma}^s & V_{AB}^s & E \\ V_{pp\sigma}^s & \varepsilon_{s1} & E & V_{AB}^s \\ V_{AB}^s & E & \varepsilon_{s2} & V_{pp\sigma}^{s'} \\ E & V_{AB}^s & V_{pp\sigma}^{s'} & \varepsilon_{s2} \end{pmatrix}, \quad (3.29)$$

where the super index  $s$  represents the perturbation with  $s$  orbitals and the matrix elements are defined by:

$$\begin{aligned} \varepsilon_{s1} &= + \frac{V_{sp\sigma}^2 (2(V_{ss\sigma} + n_{ly} n_y V_{ss\sigma})^2 - (1 + n_{ly}^2 n_y^2) \varepsilon_s^2)}{-4V_{ss\sigma}^2 \varepsilon_s + \varepsilon_s^3}, \\ \varepsilon_{s2} &= - \frac{V_{sp\sigma}^2 (-2(-1 + n_{ly} n_y)^2 V_{ss\sigma}^2 + (1 + n_{ly}^2 n_y^2) \varepsilon_s^2)}{-4V_{ss\sigma}^2 \varepsilon_s + \varepsilon_s^3}, \\ V_{pp\sigma}^s &= V_{pp\sigma} + \frac{(-1 + n_{ly} n_y)^2 V_{sp\sigma}^2 V_{ss\sigma}}{4V_{ss\sigma}^2 - \varepsilon_s^2}, & V_{pp\sigma}^{s'} &= V_{pp\sigma} + \frac{(V_{sp\sigma} + n_{ly} n_y V_{sp\sigma})^2 V_{ss\sigma}}{4V_{ss\sigma}^2 - \varepsilon_s^2}, \\ V_{AB}^s &= V_{AB} + \frac{(-1 + n_{ly}^2 n_y^2) V_{sp\sigma}^2 V_{ss\sigma}}{4V_{ss\sigma}^2 - \varepsilon_s^2}, & E &= - \frac{2(-1 + n_{ly}^2 n_y^2) V_{sp\sigma}^2 V_{ss\sigma}}{-4V_{ss\sigma}^2 \varepsilon_s + \varepsilon_s^3}. \end{aligned} \quad (3.30)$$

The Hamiltonian in the reciprocal space, considering the nearest first neighbors contributions, can be calculated with a procedure similar to the one shown in Subsec. 3.1.3 (Eqs. (3.5) to (3.10) ), and is given by:

$$H^s(\mathbf{k}) = \begin{pmatrix} \varepsilon_{s1} & V_{pp\sigma}^s g(\mathbf{k}) & V_{AB}^s f(\mathbf{k}) & Ef^*(\mathbf{k})g(\mathbf{k}) \\ V_{pp\sigma}^s g^*(\mathbf{k}) & \varepsilon_{s1} & Ef(\mathbf{k})g^*(\mathbf{k}) & V_{AB}^s f^*(\mathbf{k}) \\ V_{AB}^s f^*(\mathbf{k}) & Ef^*(\mathbf{k})g(\mathbf{k}) & \varepsilon_{s2} & V_{pp\sigma}^{s'} g^*(\mathbf{k}) \\ Ef(\mathbf{k})g^*(\mathbf{k}) & V_{AB}^s f(\mathbf{k}) & V_{pp\sigma}^{s'} g(\mathbf{k}) & \varepsilon_{s2} \end{pmatrix}. \quad (3.31)$$

Using the matrix Eq. (3.31), we find the electronic band structure of phosphorene perturbed by  $s$  orbitals around the vicinity of the high symmetry points  $\Gamma$  and  $S$ , which is shown in Fig. 3.4. The expressions of the eigenvalues obtained with Eq. 3.31 contain a large number of terms, which makes difficult to extract information about the hybridization between orbitals that contribute to the shape of the bands in the mentioned symmetry points, therefore we do not include them in this work. The values of the SK parameters used to obtain the bands are defined in Table. 3.10.

Table 3.10: Table with the Tigh-Binding parameters used for the adjustment with the DFT bands, for the model of  $|\phi\rangle$  perturbed by  $s$  orbitals. Where  $V_{sp\sigma}$ ,  $V_{ss\sigma}$ ,  $\varepsilon_{sp}$ ,  $V_{pp\sigma}$ , and  $V_{pp\pi}$  represents the SK parameters used for the calculation of the hopping integrals.

Parameter	Value (eV)	Values of Ref. [32] (eV)
$V_{sp\sigma}$	2.12	2.39
$V_{ss\sigma}$	-0.5	-1.59
$\varepsilon_{sp}$	-8.6	-8.8
$V_{pp\sigma}$	3.04	4.03
$V_{pp\pi}$	-1	-1.14

As we can see in Fig. 3.4a around the  $\Gamma$  point our bands, represented by magenta (solid) lines, reproduce very well the shape of the conduction and the valence bands compared with the fit model of DFT from [30] blue (-dashed-) lines. The value of the band-gap does not change significantly and is 2.14 eV (see Fig. 3.4a). On the other hand, around the  $S$  point (see Fig. 3.4b), we can see that our model does not give the correct band-gap, but reproduce very well, as before, the shape of the bands given by the DFT model. In summary, we can observe that the perturbation with  $s$  orbitals, does not affect significantly the shape of the bands. Again, we compared the Slater and Koster parameters obtained including the  $s$  orbitals with the ones



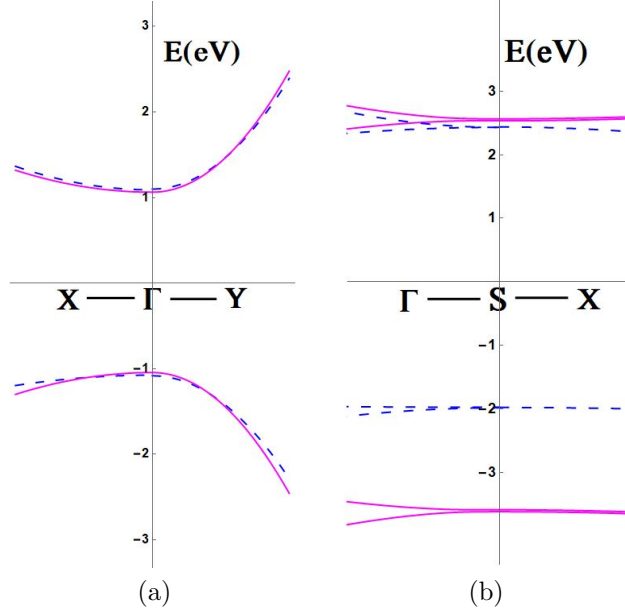


Figure 3.4: Band structure of phosphorene with  $|\phi\rangle$  orbitals perturbed by  $s$  orbitals. (a) Valence and conduction bands around  $\Gamma$  point in the  $X - \Gamma - Y$  directions. (b) Valence and conduction bands around the S point in the  $\Gamma - S - X$  directions. In both cases, the blue (-dashed-) lines represent the DFT fitting taken from [30], and the magenta (solid) lines represent the eigenvalues obtained by our tight-binding model from Eq. (3.31).

reported by Menezes *et. al.* (Table 1 in reference [32]), finding that they are very close.

After having developed an analytical Tight-Binding model based on the Slater and Koster approximation for the phosphorene structure, it could be evidenced that: The inclusion of the  $|\theta\rangle$  and  $s$  orbitals in a perturbative way does not change significantly the shape of the bands around the  $\Gamma$  and S points, with respect to the model with only  $|\phi\rangle$  orbitals. Therefore, this last model is sufficiently complete to describe the electronic properties of phosphorene around the mentioned high symmetry points shown by the DFT calculations [30]. Finally, it is important to mention that in the model described here, the effect of the overlap parameters is not considered. As a future work, the effect of these parameters can be included in the model in order to improve the fit of the bands to those obtained from DFT calculations.

# Chapter 4

## Conclusions and future work

An analytical tight-binding model for phosphorene was introduced. The model is based in terms of the Slater and Koster parameters, and with a rotating basis of  $|\phi\rangle$  orbitals that contain only  $p_y$  and  $p_z$  atomic orbitals. It is shown that this minimal model suffices to reproduce and explain the main characteristics of the electronic band structure of phosphorene around the  $\Gamma$  and S high symmetry points. The analytical expressions obtained for the eigenvalues of the Hamiltonian allow us to explain the specific dependence with the hybridizations between different orbitals from the atoms in the crystal lattice. The expressions also explain the origin of the band's asymmetry around the  $\Gamma$  point, which is strongly dependent on the SK parameter  $V_{AB}$ , representing the hybridization of the  $|\phi\rangle$  orbitals between the A and B atoms.

With this model, we have also reproduced other characteristics of the bands like the band gap of 2.19 eV which is very close to the reported experimentally of about 2 eV, and by DFT of 2.17 eV. The shape of the bands around the two mentioned high symmetry points is also well fitted to the DFT bands. Finally, the SK parameters obtained are very close to the ones reported in the literature. The inclusion of other orbitals in the model, like the  $|\theta\rangle$  and  $s$  orbitals, does not change significantly the shape of the bands, therefore, the model only with  $|\phi\rangle$  orbitals is sufficiently complete to describe the physics around the  $\Gamma$  and S points.

The Hamiltonian model presented in this thesis can be used in future works as an input to a more complete model that includes spin-orbit coupling, spin relaxation, the study of the proximity effects, among others. In the same way, the analytical terms found can be helpful for the experimental study of the electronic, transport, magneto-transport properties, Landau levels, tunable optical properties, layered controlled anisotropic excitons, quantum oscillations in few layers, etc; in phosphorene, since they allow to have simple expressions that detail the trend or behavior of the material depending on

the hybridizations between orbitals. Finally, a better fitting of the bands can be accomplished by including the overlapping parameters into the model.

# Appendix A

## Continuum Hamiltonian around the $\Gamma$ point

We can take the Hamiltonian from the equation Eq. (3.11) and approximate the respective spectral functions,  $f(\mathbf{k})$  and  $g(\mathbf{k})$ , at low energies around the  $\Gamma$  point, taking up to second order in  $k_x$  and  $k_y$ :

$$\begin{aligned}
 f(\mathbf{k}) &= \sum_{l=1}^2 e^{i\mathbf{k}\cdot\delta_{ABl}} = 2e^{ik_y y} \cos\left(\frac{bk_x}{2}\right), \\
 &\approx 2\left(1 + iyk_y - \frac{y^2 k_y^2}{2}\right) \left(1 - \frac{b^2 k_x^2}{8}\right) \approx \left(2 - \frac{b^2 k_x^2}{4} + 2ik_y y - k_y^2 y^2\right), \\
 g(\mathbf{k}) &\approx \left(1 - ihk_y - \frac{h^2 k_y^2}{2}\right)
 \end{aligned} \tag{A.1}$$

Replacing the approximated spectral functions from the equation Eq. (A.1) into the Hamiltonian Eq. (3.11) we have

$$H^\phi(\mathbf{k}) \approx \begin{pmatrix} 0 & V_{pp\sigma} \left(1 - ihk_y - \frac{h^2 k_y^2}{2}\right) & V_{AB} \left(2 - \frac{b^2 k_x^2}{4} + 2ik_y y - k_y^2 y^2\right) & 0 \\ V_{pp\sigma} \left(1 + ihk_y - \frac{h^2 k_y^2}{2}\right) & 0 & 0 & V_{AB} \left(2 - \frac{b^2 k_x^2}{4} - 2ik_y y - k_y^2 y^2\right) \\ V_{AB} \left(2 - \frac{b^2 k_x^2}{4} - 2ik_y y - k_y^2 y^2\right) & 0 & 0 & V_{pp\sigma} \left(1 + ihk_y - \frac{h^2 k_y^2}{2}\right) \\ 0 & V_{AB} \left(2 - \frac{b^2 k_x^2}{4} + 2ik_y y - k_y^2 y^2\right) & V_{pp\sigma} \left(1 - ihk_y - \frac{h^2 k_y^2}{2}\right) & 0 \end{pmatrix}. \tag{A.2}$$

36 APPENDIX A. CONTINUUM HAMILTONIAN AROUND THE  $\Gamma$  POINT

The eigenvalues calculated from Eq. (A.2) around the  $\Gamma$  point, in the directions in  $\Gamma - X$  and  $\Gamma - Y$  are:

$$\begin{aligned} \varepsilon_{\Gamma X \pm} &= \pm \left( 2 - \frac{b^2 k_x^2}{4} \right) V_{AB} \pm V_{pp\sigma}, & \varepsilon_{\Gamma X \pm} &= \mp \left( 2 - \frac{b^2 k_x^2}{4} \right) V_{AB} \pm V_{pp\sigma}, \\ \varepsilon_{\Gamma Y \pm} &= \pm \sqrt{(-2V_{AB} + V_{pp\sigma})^2} \pm \frac{V_{AB} V_{pp\sigma} (h + y)^2 k_y^2}{\sqrt{(-2V_{AB} + V_{pp\sigma})^2}}, \\ \varepsilon_{\Gamma Y \pm} &= \pm \sqrt{(2V_{AB} + V_{pp\sigma})^2} \mp \frac{V_{AB} V_{pp\sigma} (h + y)^2 k_y^2}{\sqrt{(2V_{AB} + V_{pp\sigma})^2}}, \end{aligned} \tag{A.3}$$

where  $\varepsilon_{\Gamma X}$  and  $\varepsilon_{\Gamma Y}$  represent the eigenvalues in the  $\Gamma - X$  and  $\Gamma - Y$  directions, and the (+) and (-) represent the conduction and the valence bands respectively. The bands that open the gap are the first one and the last one equations from Eq. (A.3). In Fig. A.1 we show the bands obtained with the eigenvalues of Eq. (A.3), compared with the bands from Eq. (3.12), and with the DFT bands reported in reference [30]. As we can see in this figure, the continuum approximation preserving up to second order in  $k_x$  and  $k_y$  fits very well with the analytical and DFT bands for general values of the wave vector.

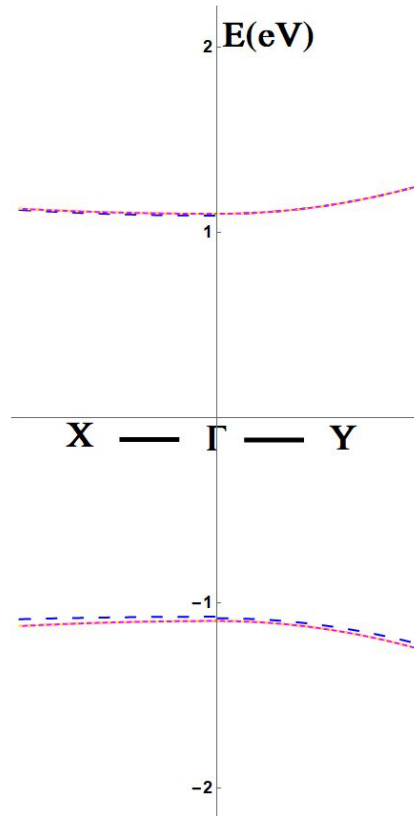


Figure A.1: Electronic band structure of phosphorene around the  $\Gamma$  point from 0 to 1 in  $\mathbf{k}$ . Valence and conduction bands around the  $\Gamma$  point in the  $\Gamma - X$  and  $\Gamma - Y$  directions. The blue (-dashed-) lines are quadratic fits of the DFT bands taken from [30], the magenta (solid) lines are the eigenvalues from Eq. (3.13) given by our tight-binding model with  $|\phi\rangle$  orbitals from Eq. (3.11), and the yellow (dotted) lines are the eigenvalues from the first and the last equations from Eq. (A.3) obtained from the continuum Hamiltonian from Eq. (A.2).

# Bibliography

- [1] J.W. You, S.R. Bongu, Q. Bao, and N.C. Panoiu. Nonlinear optical properties and applications of 2d materials: theoretical and experimental aspects. *Nanophotonics*, 8(1):63–97, 2019.
- [2] C. N. R. Rao, Kanishka Biswas, K. S. Subrahmanyam, and A. Govindaraj. Graphene, the new nanocarbon. *J. Mater. Chem.*, 19:2457–2469, 2009.
- [3] Minjie Wang and Eui-Hyeok Yang. Terahertz applications of 2d materials: Graphene and beyond. *International Journal of Smart and Nano Materials*, 15:107, 04 2018.
- [4] Liangzhi Kou, Changfeng Chen, and Sean C. Smith. Phosphorene: Fabrication, properties and applications, 2015.
- [5] Zhaogang Nie, Run Long, Linfeng Sun, Chung-Che Huang, Jun Zhang, Qihua Xiong, Daniel W. Hewak, Zexiang Shen, Oleg V. Prezhdo, and Zhi-Heng Loh. Ultrafast carrier thermalization and cooling dynamics in few-layer mos<sub>2</sub>. *ACS Nano*, 8(10):10931–10940, 2014. PMID: 25268655.
- [6] Zhipei Sun, Tawfique Hasan, Felice Torrisi, Daniel Popa, Giulia Privitera, Fengqiu Wang, Francesco Bonaccorso, Denis M. Basko, and Andrea C. Ferrari. Graphene mode-locked ultrafast laser. *ACS Nano*, 4(2):803–810, 2010. PMID: 20099874.
- [7] Manish Chhowalla, Zhongfan Liu, and Hua Zhang. Two-dimensional transition metal dichalcogenide (tmd) nanosheets. *Chem. Soc. Rev.*, 44:2584–2586, 2015.
- [8] Sreekanth J. Varma, Jitesh Kumar, Yang Liu, Katherine Layne, Jingjie Wu, Chenglu Liang, Yusuke Nakanishi, Amir Aliyan, Wei Yang, Pulickel M. Ajayan, and Jayan Thomas. 2d tms<sub>2</sub> layers: A superior nonlinear optical limiting material. *Advanced Optical Materials*, 5(24):1700713, 2017.

- [9] Haitao Chen, Vincent Corbaliou, A. Solntsev, D. Choi, M. Vincenti, D. de Ceglia, C. De Angelis, Yuerui Lu, and D. Neshev. Enhanced second-harmonic generation from two-dimensional mose2 on a silicon waveguide. *Light, Science & Applications*, 6, 2017.
- [10] T. Zhao, M. Hu, R. Zhong, X. Chen, P. Zhang, S. Gong, C. Zhang, and S. Liu. Terahertz generation from graphene surface plasmon polaritons excited by a cyclotron electron beam. In *2016 41st International Conference on Infrared, Millimeter, and Terahertz waves (IRMMW-THz)*, pages 1–2, 2016.
- [11] Huakang Yu, Deep Talukdar, Weigao Xu, Jacob B. Khurgin, and Qihua Xiong. Charge-induced second-harmonic generation in bilayer wse2. *Nano Letters*, 15(8):5653–5657, 2015. PMID: 26203670.
- [12] Antti J. Karttunen, Mikko Linnolahti, and Tapani A. Pakkanen. Structural principles of polyhedral allotropes of phosphorus. *ChemPhysChem*, 9(17):2550–2558, 2008.
- [13] M. Averbuch-pouchot and A. Durif. *Topics In Phosphate Chemistry*. World Scientific Publishing Company, 1996.
- [14] Lihui Zhang, Hongyang Huang, Bo Zhang, Mengyue Gu, Dan Zhao, Xuewen Zhao, Longren Li, Jun Zhou, Kai Wu, Yonghong Cheng, and Jinying Zhang. Structure and properties of violet phosphorus and its phosphorene exfoliation. *Angewandte Chemie International Edition*, 59(3):1074–1080, 2020.
- [15] M. Zeldin. *Inorganic and organometallic polymers*. AccessScience. McGraw-Hill Education., 2020.
- [16] Samira Bagheri, Negar Mansouri, and Ermia Aghaie. Phosphorene: A new competitor for graphene. *International Journal of Hydrogen Energy*, 41(7):4085–4095, 2016.
- [17] Xi Ling, Han Wang, Shengxi Huang, Fengnian Xia, and Mildred S. Dresselhaus. The renaissance of black phosphorus. *Proceedings of the National Academy of Sciences of the United States of America*, 112(15):4523–4530, April 2015. Publisher Copyright: © 2015, National Academy of Sciences. All rights reserved. Copyright: Copyright 2015 Elsevier B.V., All rights reserved.



- [18] Vy Tran, Ryan Soklaski, Yufeng Liang, and Li Yang. Layer-controlled band gap and anisotropic excitons in few-layer black phosphorus. *Phys. Rev. B*, 89:235–319, Jun 2014.
- [19] A. Brown and S. Rundqvist. Refinement of the crystal structure of black phosphorus. *Acta Crystallographica*, 19(4):684–685, Oct 1965.
- [20] L. Li, Y. Yu, G. J. Ye, Q. Ge, X. Ou, H. Wu, D. Feng, X. H. Chen, and Y. Zhang. Black phosphorus field-effect transistors. *Nature nanotechnology*, 9:372–377, 2014.
- [21] Han Liu, Yuchen Du, Yexin Deng, and Peide D. Ye. Semiconducting black phosphorus: synthesis, transport properties and electronic applications. *Chem. Soc. Rev.*, 44:2732–2743, 2015.
- [22] J. Wittig and B. T. Matthias. Superconducting phosphorus. *Science*, 160(3831):994–995, 1968.
- [23] Haruki Kawamura, Ichimin Shirotnani, and Kyoji Tachikawa. Anomalous superconductivity and pressure induced phase transitions in black phosphorus. *Solid State Communications*, 54(9):775–778, 1985.
- [24] Han Liu, Adam T. Neal, Zhen Zhu, Zhe Luo, Xianfan Xu, David Tománek, and Peide D. Ye. Phosphorene: An unexplored 2d semiconductor with a high hole mobility. *ACS Nano*, 8(4):4033–4041, 2014. PMID: 24655084.
- [25] Liangbo Liang, Jun Wang, Wenzhi Lin, Bobby G. Sumpter, Vincent Meunier, and Minghu Pan. Electronic bandgap and edge reconstruction in phosphorene materials. *Nano Letters*, 14(11):6400–6406, 2014. PMID: 25343376.
- [26] Xiaomu Wang, Aaron Jones, Kyle Seyler, Vy Tran, Yichen Jia, Huan Zhao, Han Wang, Li Yang, Xiaodong Xu, and Fengnian Xia. Highly anisotropic and robust excitons in monolayer black phosphorus. *Nature nanotechnology*, 10, 11 2014.
- [27] Alexandra Carvalho, Min Wang, Xi Zhu, Aleksandr S. Rodin, Haibin Su, and Antonio H. Castro Neto. Phosphorene: from theory to applications. *Nature Reviews Materials*, 1(11):16061, November 2016.
- [28] Sheneve Z. Butler, Shawna M. Hollen, Linyou Cao, Yi Cui, Jay A. Gupta, Humberto R. Gutiérrez, Tony F. Heinz, Seung Sae Hong, Jiaying Huang, Ariel F. Ismach, Ezekiel Johnston-Halperin, Masaru Kuno,

- Vladimir V. Plashnitsa, Richard D. Robinson, Rodney S. Ruoff, Sayeef Salahuddin, Jie Shan, Li Shi, Michael G. Spencer, Mauricio Terrones, Wolfgang Windl, and Joshua E. Goldberger. Progress, challenges, and opportunities in two-dimensional materials beyond graphene. *ACS Nano*, 7(4):2898–2926, 2013. PMID: 23464873.
- [29] W.A. Harrison. *Electronic Structure and the Properties of Solids: The Physics of the Chemical Bond*. Dover Books on Physics. Dover Publications, 2012.
- [30] Marcin Kurpas, Martin Gmitra, and Jaroslav Fabian. Spin-orbit coupling and spin relaxation in phosphorene: Intrinsic versus extrinsic effects. *Physical Review B*, 94(15), Oct 2016.
- [31] Andrea Lorenzoni, Matteo Baldoni, Elena Besley, and Francesco Mercuri. Noncovalent passivation of supported phosphorene for device applications: from morphology to electronic properties. *Phys. Chem. Chem. Phys.*, 22:12482–12488, 2020.
- [32] Marcos G. Menezes and Rodrigo B. Capaz. Tight binding parametrization of few-layer black phosphorus from first-principles calculations. *Computational Materials Science*, 143:411–417, 2018.
- [33] Ting Hu, Yang Han, and Jinming Dong. Mechanical and electronic properties of monolayer and bilayer phosphorene under uniaxial and isotropic strains. *Nanotechnology*, 25(45):455703, oct 2014.
- [34] Jingsi Qiao, Xianghua Kong, Zhi-Xin Hu, Feng Yang, and Wei Ji. High-mobility transport anisotropy and linear dichroism in few-layer black phosphorus. *Nature Communications*, 5(1), Jul 2014.
- [35] Z. S. Popović, Jamshid Moradi Kurdestany, and S. Satpathy. Electronic structure and anisotropic rashba spin-orbit coupling in monolayer black phosphorus. *Phys. Rev. B*, 92:035135, Jul 2015.
- [36] Paulo E. Faria Junior, Marcin Kurpas, Martin Gmitra, and Jaroslav Fabian. k·p theory for phosphorene: Effective g-factors, landau levels, and excitons. *Physical Review B*, 100(11), Sep 2019.
- [37] Shuhei Fukuoka, Toshihiro Taen, and Toshihito Osada. Electronic structure and the properties of phosphorene and few-layer black phosphorus. *Journal of the Physical Society of Japan*, 84, 07 2015.

- [38] Narges Kafaei, Khadijeh Beiranvand, Mohammad Sabaeian, Abdolmohammad Ghalambor Dezfuli, and Han Zhang. Spin-dependent k.p hamiltonian of black phosphorene based on löwdin partitioning method. *Journal of Applied Physics*, 124(3):035702, 2018.
- [39] C. Kittel. *Introduction to Solid State Physics*. Wiley, 2004.
- [40] J. C. Slater and G. F. Koster. Simplified lcao method for the periodic potential problem. *Phys. Rev.*, 94:1498–1524, Jun 1954.
- [41] W. E. Pickett. "tight binding" method: Linear combination of atomic orbitals (lcao). *UCDavis*, 11 2006.
- [42] Edward McCann and Mikito Koshino. The electronic properties of bilayer graphene. *Reports on Progress in Physics*, 76(5):056503, apr 2013.
- [43] Edward McCann. *Electronic properties of monolayer and bilayer graphene*, pages 237–275. NanoScience and Technology. Springer Verlag, 2012.
- [44] Mervyn Roy. The tight binding method. *Rutgers University*, 05 2015.
- [45] Jaroslav Fabian. Spin-orbit coupling in graphene: from single layers to graphite. *Universität Regensburg*, 03 2011.
- [46] Mayra Peralta, Ernesto Medina, and Francisco Mireles. Proximity-induced exchange and spin-orbit effects in graphene on ni and co. *Phys. Rev. B*, 99:195452, May 2019.